Decadal modulations of interhemispheric global atmospheric circulations and monsoons by the South Atlantic Meridional Overturning Circulation

Hosmay Lopez[1,2], Shenfu Dong[1,2], Sang-Ki Lee[1,2] and Gustavo Goni[2]

[1]Cooperative Institute for Marine and Atmospheric Studies, University of Miami, Miami, Florida

[2]Atlantic Oceanographic and Meteorological Laboratory, NOAA, Miami, Florida

Abstract

This study presents a physical mechanism on how low frequency variability of the South Atlantic Meridional Heat Transport (SAMHT) may influence decadal variability of atmospheric circulation. A multi-century simulation of a coupled general circulation model is used as basis for the analysis. The highlight of our findings is that multi-decadal variability of SAMHT plays a key role in modulating global atmospheric circulation via its influence on interhemispheric redistributions of momentum, heat, and moisture. Weaker SAMHT at 30°S produces anomalous ocean heat divergence over the South Atlantic, resulting in negative ocean heat content anomalies about 15-20 years later. This forces a thermally direct anomalous interhemispheric Hadley circulation, transporting anomalous atmospheric heat from the Northern Hemisphere (NH) to the Southern Hemisphere (SH) and moisture from the SH to the NH, thereby modulating global monsoons. Further analysis shows that anomalous atmospheric eddies transport heat northward in both hemispheres, producing eddy heat flux convergence (divergence) in the NH (SH) around 15 - 30°, reinforcing the anomalous Hadley circulation. The effect of eddies on the NH (SH) poleward of 30° depict heat flux divergence (convergence), which must be balanced by sinking (rising) motion, consistent with a poleward (equatorward) displacement of the jet stream.

This study illustrates that decadal variations of SAMHT could modulate the strength of global monsoons with 15 - 20 years of lead-time, suggesting that SAMHT is a potential predictor of global monsoon variability. A similar mechanistic link exists between the North Atlantic Meridional Heat Transport (NAMHT) at 30°N and global monsoons.

Corresponding author address: Hosmay Lopez UM/CIMAS/RSMAS and NOAA/AOML/PHOD 4301 Rickenbacker Causeway, Miami, FL 33149, USA. E-mail: hlopez@rsmas.miami.edu

1. Introduction

The Atlantic Meridional Overturning Circulation (AMOC) is characterized by northward-flowing warm water in the upper ocean and a southward compensating flow of cold water at depth (e.g., Broecker 1991; Lumpkin and Speer 2007). There have been numerous efforts to understand the role of the AMOC as a potential predictor of decadal climate variability, motivated partly by its inherent relationship with the North Atlantic sea surface temperature (SST, e.g., Latif et al. 2006; Corti et al. 2012). Therefore, the majority of efforts to understand the dynamics of the AMOC and its climate impacts have focused on the North Atlantic. The mechanism for the North Atlantic multi-decadal SST variability, also known as the Atlantic Multidecadal Oscillation (AMO, e.g., Enfield et al. 2001), has been shown to be modulated by AMOC changes (e.g., Latif et al. 2004; Knight et al. 2005; Zhang et al. 2013) and linked to decadal variability of the North Atlantic Oscillation (NAO, e.g., Sun et al. 2015).

Sun et al. (2015) suggested a three-way interaction among the NAO, AMOC and AMO with the NAO leading the AMO by 15-20 years, while the AMO provides a delayed negative feedback to the NAO. Latif et al. (2000) also found a similar relationship between decadal variability of the NAO and North Atlantic SSTs. Drevillon et al. (2001) argued that SST anomalies over the North Atlantic induce atmospheric stationary waves, which are strengthened by transient eddies. These studies collectively showed that the AMO influences and also is influenced by the strength of the AMOC and associated Meridional Heat Transport (MHT) suggesting a delayed advective oscillation (Lee and Wang 2010).

North Atlantic SST anomalies associated with the AMO significantly influence climate anomalies over North America, West Africa and Europe (e.g., Enfield et al. 2001; Kushmir et al. 2002; Rodwell and Folland 2003; Knight et al. 2006; Zhang and Delworth 2006; Ting et al.

2011; Tung and Zhou 2013; Peings and Magnusdottir 2014). Several studies have suggested that the AMO's impact on climate is largely forced in the low latitudes (e.g., Sutton and Hodson 2005). By modulating the strength and meridional location of the Atlantic Intertropical Convergence Zone (ITCZ), the AMO can force extra-tropical atmospheric stationary waves to influence summertime Western Europe temperature anomalies (Ambrizzi et al. 1995; Cassou et al. 2004; Cassou et al. 2005). Some studies argue that the meridional ITCZ shifts are also linked to sea ice concentrations over the North Atlantic (Chiang and Bitz 2005), fresh water fluxes into the North Atlantic (Stouffer et al. 2006; Zhang and Delwoth 2005) and aerosol-induced heating/cooling over the high latitudes in the northern hemisphere (NH) (e.g., Yoshimori and Broccoli 2008). Kang et al. (2009) proposed that antisymmetric interhemispheric heating in high latitudes linked to AMOC shutdown could control the location of the ITCZ, and that its shift could be related to changes in atmospheric energy transport. Consistently, Frierson et al. (2013) argued that oceanic MHT contributes significantly to the asymmetry in precipitation by transporting heat northward, which moves the tropical rainband and ITCZ northward. Several studies argue for the existence of two stable AMOC states, an "on" and an "off" state, from theoretical arguments (Stommel 1961), modeling studies (Manabe and Stouffer 1988; Lenton et al. 2009; Hawkins et al. 2011), and paleoclimate records (Broecker et al. 1985; Clark et al. 2002). Recent numerical model 21st Century projections suggest a considerable weakening of the AMOC (Kriegler et al. 2009; Cheng et al. 2013). Zhang and Delworth (2005) showed that a substantial weakening of the AMOC results in a southward shift of the ITCZ, with a weakening of the Indian and Asian summer monsoons, and an El Niño-like pattern in the southeastern Pacific.

As briefly reviewed above, the majority of efforts to understand the dynamics of the AMOC and its climate impact are focused on the North Atlantic. Recently, the research community started investigating and assessing the role of the South Atlantic on climate. Direct or indirect measurements from in-situ observations have shown a wide range of AMOC values at 35°S from -0.24 PW (de las Heras and Schlitzer 1999) to 0.55 PW (Dong et al. 2011) and to 0.94 PW (Saunders and King 1995). The AMOC over the South Atlantic Ocean is unique, in that it is the only major ocean basin that transports heat from the pole towards the equator (Talley 2003). Recent studies have suggested the possibility of the anomalous AMOC and MHT originating from the inter-ocean transport from the Indian Ocean (e.g., Biastoch et al. 2009; Lee et al. 2011).

The South Atlantic Ocean is characterized by complex and unique ocean dynamic processes, which are important to the global distribution of energy. For example, the Malvinas-Brazil Confluence (Garzoli and Garraffo 1989; Goni et al. 2011) plays a critical role in the exchange of water masses between the subpolar and the subtropical regions. The Agulhas leakage, , which is the main balance for the outflow of North Atlantic deep water (Gordon 1985; Sloyan and Rintoul 2001) has the potential for modifying the long-term AMOC response that could impact global atmospheric circulation and climate (Weijier et al. 1999; Sloyan and Rintoul 2001; Garzoli and Matano 2011). Dong et al. (2011) pointed out that interannual and longer-term decadal changes in AMOC and MHT over the South Atlantic are due to advective heat convergence from inter-basin heat exchange, mainly through the Agulhas leakage. Lee et al. (2011) showed that this inter-basin heat transport has increased since the 1950s and contributed to the significant increase in Atlantic Ocean heat content.

Here, we present a physical mechanism by which the South Atlantic Meridional Heat Transport (SAMHT) modulates changes in the atmospheric circulation. Our hypothesis is that low-frequency variations in SAMHT influence interhemispheric atmospheric heat and moisture transport through slow changes in the upper ocean heat content of the South Atlantic. Our study shows that this upper ocean heat content anomaly, linked to meridional heat convergence/divergence, forces a thermally direct anomalous interhemispheric Hadley circulation as well as atmospheric eddy-driven circulations in both hemispheres, and thus shifts the location and strength of the ITCZ and modulates monsoonal circulations.

The motivation of this work is to enhance our understanding of the SAMHT and its potential role in predicting global and regional climate variability. In this work, we show that a weaker-than-normal SAMHT leads to a strengthening and northward shift of the ITCZ about 15 - 20 years later. This is possible through a modification of the zonal mean atmospheric Hadley circulation by anomalous negative heat content over the tropical South Atlantic, with potential implications on the global monsoon circulations. For this, multi-century output from a Coupled General Circulation Model (CGCM) is analyzed. Basic information about the model is presented in section 2. Multidecadal variability of the Atlantic Ocean transports is discussed in section 3. Section 4 discusses the atmospheric response to changes in SAMHT. Section 5 presents the SAMHT modulation of precipitation and monsoon circulations. Section 6 investigates the relative roles of SAMHT and the North Atlantic MHT (NAMHT). A summary is presented in section 7, with discussion of a possible mechanism for multidecadal ocean-atmosphere interactions. Concluding remarks are presented in section 8.

2. Data and Coupled Model

The global estimate of precipitation for the period from January 1950 to December 2011 is taken from the Global Precipitation Climatology Centre (GPCC, Becker et al. 2013) on a 1° grid. Estimates for the AMOC and MHT at 26°N are from direct measurements from the Rapid Climate Change Meridional overturning Circulation and Heat flux array (RAPID-MOCHA) observing system (Cunningham et al. 2007). The estimates of the MHT at 34°S are derived from expendable bathythermograph (XBTs) and Argo float measurements (Dong et al. 2009, 2014).

The CGCM used in this work is the Community Earth System Model (CESM1) from the National Center for Atmosphere Research (NCAR). This earth system model consists of atmosphere, land, ocean, glaciers, and sea ice components, all linked by a flux coupler. The coupler exchanges daily information among the components interactively. The atmospheric component is the Community Atmosphere Model version 5 (CAM5). It has 30 vertical levels with horizontal resolution of 1.25° longitude by 0.94° latitude. The dynamical core uses the finite volume formulation. It employs an improved deep convection scheme by inclusion of sub-grid convective momentum transport and a more realistic dilution approximation for the calculation of convective available potential energy (Neale et al. 2008). The ocean model component uses the Parallel Ocean Program version 2 (POP2) (Danabasoglu et al. 2012). It has a 1° horizontal resolution with 60 vertical levels. This updated version of POP includes a simplified version of the near boundary eddy flux parameterization of Ferrari et al. (2008), vertically-varying isopycnal diffusivity coefficients (Danabasoglu and Marshall 2007), an abyssal tidally-driven mixing parameterization, modified anisotropic horizontal viscosity coefficients (Jochum et al. 2008), and a modified K-Profile Parameterization with horizontally varying background vertical diffusivity and viscosity coefficients (Jochum 2009).

159 An extensive evaluation of the ocean component of the model over the South Atlantic
160 and Southern Ocean was discussed in Weijer et al. (2012). There, they showed that simulated
161 ocean variability over the southern hemisphere (SH) is dominated by the South Annular Mode,
162 which is consistent with observations. The model also reproduces the correct characteristics of
163 the frontal zone associated with the Antarctic Circumpolar Current and the SH inter-basin ocean
164 exchanges to a reasonable degree. However, the model struggles in representing the correct
165 location of the Brazil-Malvinas current confluence, which is displaced southward compared to
166 observations. Also, the Agulhas leakage is too strong, and is zonally oriented compared to
167 satellite observational estimates.

168 In order to have a robust estimate of the mean climate and variability, we evaluate 1,100
169 years of pre-industrial simulation using CESM1. More detailed discussions on this model can be
170 found in Kay et al. (2014). All choices of fields analyzed are from monthly mean model outputs.
171 Although the model does not show any long-term climate drift, all data are detrended before
172 analysis. The model run is a pre-industrial simulation with atmospheric composition from 1850,
173 since we are mainly interested in internal variability in this study.

174

175 **3. Results**

176 **a. South Atlantic Meridional Heat Transport**

177 Figure 1 shows the mean ocean MHT in the Atlantic derived from CESM1 and from
178 various observational and reanalysis products. The mean MHT over the Atlantic Ocean is well
179 represented in CESM1. Its amplitude is larger than estimates from the European Center for
180 Medium Range Weather Forecast (ECMWF) and comparable with that derived from the
181 National Center for Environmental prediction (NCEP) reanalysis (Trenberth et al. 2001).

Trenberth et al. (2001) found that ocean MHT estimates from NCEP were in good agreement with direct ocean measurements and coupled models. In contrast, the ECMWF-derived MHT estimates are deficient due to problems with changes in the observing system, specifically satellite data. The mean MHT of 1.18 PW at 26°N from CESM1 is comparable with the 1.33 PW estimated from the RAPID-MOCHA observing system (Johns et al. 2011). The observational-based MHT estimate at 34°S (e.g., Dong et al. 2009; Dong et al., 2015) is also well captured by CESM1. Overall, the MHT over the Atlantic Ocean is well represented by the model.

An index for the SAMHT is constructed here by computing the anomalous MHT across the Atlantic basin at 30°S, where the anomaly is obtained by removing the seasonal cycle of the transport and any trend that might be present. The SAMHT is further decomposed into the Ekman and geostrophic components. The Ekman component is estimated using monthly mean zonal wind stress from CESM1, whereas the geostrophic term is simply taken as the difference between the total and Ekman component.

There are two dominant power spectral peaks at frequencies of about 30 and 60 years in the simulated MHT (not shown). In general, the power spectrum of SAMHT is dominated by low frequencies with a red-spectrum structure. The reddening is mostly from the geostrophic component, where most of the power occurs on multi-decadal timescales. The Ekman component has power at almost all frequencies, although the 60-year spectral peak is also prominent there. The multi-decadal frequencies (i.e., periods higher than 11 years) contain about 53% of the total SAMHT variance. For the Ekman (geostrophic) component, the variance explained by the multi-decadal frequencies accounts for about 35% (83%) of its total variance. Therefore, it is appropriate to focus on the low-frequency variability of SAMHT. For this, an 11-year running average is performed on the interannual anomaly of SAMHT, and shown in Fig. 2 as the time

205 series for each component for the 1,100 model years. Note that the Ekman and geostrophic
206 components have about the same amplitude as the total SAMHT. Overall, the geostrophic
207 component explains most of the low-frequency variance of the total SAMHT, consistent with the
208 spectral peaks mentioned earlier. It is also evident that the geostrophic component tends to
209 redden the spectrum of the total SAMHT, whereas the Ekman is comprised of higher
210 frequencies, even after the 11-year running average is applied. The results presented here are
211 largely independent of the choice of the filtering window used, which ranges from 7 to 15 years.
212 The time series shown in Fig. 2a is used in this work as the basis for studying the
213 relationships between the SAMHT and global climate variability. Those relationships will be
214 assessed via composite analyses of the state of the SAMHT. A strong (weak) SAMHT is defined
215 as periods where SAMHT is one standard deviation above (below) the mean value. Here, a
216 reliable composite difference (i.e., weak minus strong SAMHT) is built from the large sample
217 size.
218
219 **b. Ocean Transport**
220 Figure 3 shows the mean and composite difference of the ocean meridional overturning
221 streamfunction for the Atlantic Ocean and the global ocean (positive streamfunction values
222 indicate clockwise circulations). Recall that the composite difference is defined by weak minus
223 strong SAMHT and referred to here as anomaly. For the AMOC (Fig.3 top), the simulated
224 AMOC is dominated by northward flow in the upper 1000 m and a return flow below. The
225 maximum streamfunction occurs at about 40°N. The anomalous AMOC (Fig. 3a) indicates that a
226 reduction in SAMHT is accompanied by a significant weakening of the AMOC extending from
227 the South Atlantic to about 45°N. The weakening in the AMOC peaks in two regions, one at

30°S and the other at about 30°N. For the global ocean (Fig. 3b), the largest value of MOC also occurs at around 40°N at 1000 m depth. The upper 700 m tropical band (30°S to 30°N) is dominated by the shallow overturning cell with upward flow near the equator, occurring predominantly in the Pacific Ocean (Klinger and Marotzke 2000; McPhaden and Zhang 2002, 2004). The anomalous overturning circulation of the global ocean is very similar in amplitude and location to that of the Atlantic, suggesting that the Atlantic basin dominates most of the anomalies at the multi-decadal timescales presented here.

c. Oscillatory mechanism

This section presents a possible mechanism by which decadal changes in SAMOC and associated SAMHT could interplay with atmospheric circulation. For this, we analyze the composite difference of Atlantic Ocean MHT, heat content (HC), heat content tendency, MHT divergence, and heat flux as a function of lead-time with respect to SAMHT. Fig. 4a shows the lead-lag composite difference of Atlantic MHT with respect to weak minus strong SAMHT. Figs. 4b, c, d and e are similar to Fig. 4a but for the surface-to-700m integrated HC, HC tendency, MHT divergence, and surface heat flux in the Atlantic Ocean. Several depths ranging from 200m down to the ocean bottom were tested to conclude that results shown here are largely independent of the choice of the integration depth for heat content calculation. There is an oscillatory pattern in the MHT (Fig. 4a) that appears to propagate from the north to the south, with North Atlantic MHT leading SAMHT by about 10 years. That is, the anomalous negative SAMHT can be traced back to the North Atlantic. Interestingly, the SAMHT leads the opposite sign in the North Atlantic MHT by about 15 years. Overall, the oscillatory pattern has a period of about 50-60 years.

By construction of the composite, the SAMHT has the most negative value at 0-lag. This is associated with a negative tendency of HC from 30°S to the equator (Fig. 4c), which leads the negative HC anomaly 10 - 20 years later (Fig. 4b). The period during and after the weakest SAMHT (e.g., 10-20 year lead) are dominated by negative (positive) HC anomaly over the SH (NH). The relationship between MHT and HC is described by (1). Assuming a perfectly enclosed basin, the zonally and vertically integrated tendency in the heat content is balanced by MHT convergence and surface heat fluxes:

$$\frac{\partial HC}{\partial t} = -\frac{\partial MHT}{\partial y} + Q_{Net} \qquad (1),$$

where the first term on the right is the convergence of the MHT. The second term is the net surface heat flux, the sum of two turbulent (latent and sensible) and two radiative (longwave and shortwave) components. The results described in Fig. 4 show an oscillatory pattern in HC over the South Atlantic (i.e., Fig. 4b) in association with SAMHT. The negative HC tendency at 0-year lag (Fig. 4c) is mainly caused by MHT divergence south of the equator (Fig. 4d). MHT convergence is balanced by heat content tendency at about 10 years prior to the weakest SAMHT between 15°N-35°N, leading to positive HC anomaly over most of the North Atlantic at 0-year lag during the weakest SAMHT. The HC anomaly in the North Atlantic Ocean is explained by MHT convergence, which is balanced by negative surface heat flux at about 10 years prior to the weakest SAMHT. The MHT convergence is mostly balanced by positive tendency of HC. The North Atlantic HC anomaly appears to be modulated by the same physical mechanism explained for the South Atlantic HC anomaly. This relationship among ocean heat content tendency, meridional heat transport convergence, and surface heat fluxes produces the meridional asymmetry in the heat content. Its impact on interhemispheric atmospheric circulation is discussed next.

Anomalous Hadley circulation corresponding to weak minus strong SAMHT is depicted in Fig. 5 as the vertically integrated mass streamfunction about the equator. Here, the direction of interhemispheric atmospheric heat transport is proportional to the mass transport with northward (southward) labeled red (blue). Note that the Atlantic Ocean heat transport (Fig. 4a) and the global atmospheric heat transport (Fig. 5) are mostly in opposite direction to each other. Prior to the weakest SAMHT (i.e., 15-lag), the atmospheric heat transport is northward. There is anomalous positive HC over most of the South Atlantic (Fig. 4b) and negative HC north of 20°N, supporting the northward atmospheric heat transport. This positive meridional gradient in oceanic HC is consistent with the anomalous Hadley circulation about 15 - 20 years after the negative SAMHT anomaly (Fig. 5, green line), which transports atmospheric heat southward. Therefore, the SAMHT leads the atmospheric heat transport response by about 15-20 years.

In summary, on decadal timescales, the interhemispheric global atmospheric mass and heat transports are directly linked to the HC of the tropical Atlantic Ocean, which is modulated by the SAMHT. The maximum northward atmospheric transport, which occurs ~15 - 20 years before the peak SAMHT, is forced by the interhemispheric gradient of Atlantic Ocean heat content (Fig. 4b). The maximum southward atmospheric transport at 0-year lag is mostly due to the anomalous positive North Atlantic Ocean heat content (maximum at about 15°N) formed by heat transport convergence 15 - 20 years earlier. Of key emphasis is what occurs after the minimum in SAMHT (i.e., after 0-year lag). The maximum southward atmospheric transport at about 15 - 20 years lead (Fig. 5) is forced by a dipole in the Atlantic Ocean heat content, induced mostly by heat transport divergence over the South Atlantic at 0-year lag. This result suggests that SAMHT could provide lead-time predictability of the state of the zonal mean atmospheric

296 circulation. For this, the next section will be focused on the 20 years delayed atmospheric
297 response to the SAMHT anomaly.
298
299 **4. Atmospheric response to SAMHT variability at 20 years lead-time**
300 Before assessing decadal changes in the global atmospheric response as a function of the
301 SAMHT, we first discuss the global distribution of heat budget for the atmosphere and ocean at
302 20 years lead-time after the anomalous SAMHT. For this, we use monthly mean radiative fluxes
303 at the top-of-the-atmosphere (TOA) consisting of net incoming solar radiation and net outgoing
304 radiation. There is large interhemispheric asymmetry in the distribution of radiative fluxes at
305 TOA, with the NH receiving a net flux of 0.14 PetaWatts and the SH losing 0.26 PetaWatts.
306 There should be a net southward heat transport by the combined ocean and atmosphere system,
307 which is shown by the hemispheric asymmetry of upper-ocean heat content in Fig. 4b. Overall,
308 there is an interhemispheric difference of about 0.4 PetaWatts in both the ocean and atmosphere
309 at 20-years lead-time after the anomalous negative SAMHT. This is roughly the same amplitude
310 as the decadal variability of SAMHT. This asymmetry must be balanced by meridional heat
311 transport. The composite difference of 500mb temperature, SST and precipitation is shown in
312 Fig. 6 at 20-year lead-time. There is tropospheric cooling (warming) in the SH (NH) associated
313 with SST anomalies of the same sign. The largest SST anomaly occurs over the South Atlantic,
314 consistent with the negative heat content there, as shown in Fig. 4b. Although the SST forcing is
315 zonally asymmetric, atmospheric eddies and westerlies homogenize it into a symmetric
316 atmospheric response (Kang et al. 2014). This creates an equatorially asymmetric precipitation
317 response in the tropics (Fig. 6c), with positive (negative) anomaly in the NH (SH). A study by
318 Sun et al. (2013) investigated the relationship between the equatorially asymmetric precipitation

and inter-hemispheric SST dipole. They found that this SST dipole arises from variability related to northward cross-equatorial ocean heat transport, with potential influence on decadal variability of tropical precipitation. The role of atmospheric eddies and the mean circulation is discussed next.

Atmospheric circulation associated with the SAMHT is assessed by analyzing the composite of the weak minus strong SAMHT, 20 years after the anomalous SAMHT. Here, a zonal mean approach is adopted to quantify the meridional fluxes of heat and moisture. Fig. 7a shows the time mean and zonal mean meridional circulation (MMC) of the atmosphere as measured by the mass streamfunction (contour) and composite difference (color). Figs. 7b and c are identical to Fig. 7a, but for the meridional heat flux and meridional moisture flux, respectively. Here, heat flux associated with MMC is defined, as $[\bar{v}][\bar{T}]$ and moisture flux is $[\bar{v}][\bar{q}]$ where v is the meridional wind, T is the temperature, and q is the specific humidity. The over bar represents time mean and brackets represent zonal mean. Northward heat and moisture flux are indicated by positive contours. The Hadley circulation is a thermally direct circulation that transports heat by its upper branch (i.e., away from the equator) and moisture by its lower branch (i.e., towards the equator). The MMC (Fig. 7a) shows anomalous negative streamfunction around the equator of the order of 10% of the mean circulation. This is indicative of strengthening (weakening) of the SH (NH) Hadley circulation about 20-years after the weakening of the SAMHT. Implications for this circulation pattern are highlighted in Figs. 7b and c in that there are anomalous interhemispheric heat and moisture fluxes (NH-to-SH heat flux and SH-to-NH moisture flux). Similar to the MMC anomalies, the composite differences in the heat and moisture fluxes are also both about 10% of the mean fluxes and are located near the equator. This anomalous circulation pattern implies strengthening of the ITCZ to the north of the

342 equator (e.g., 15°N) where moisture flux convergences at lower levels and heat flux divergence
343 at upper levels increase the Convective Available Potential Energy (CAPE) and thus strengthen
344 the NH summer monsoon via the so-called interhemispheric teleconnection mechanism (e.g., Lee
345 et al. 2013).

346 The MMC is well known to be crucial in heat and moisture distribution from equator to
347 higher latitudes. However, atmospheric eddies, stationary and transient, are also important in
348 heat distribution at mid-latitudes. In a zonal mean state, stationary and transient eddy heat flux is
349 toward the poles. These eddies result from the unstable equator-to-pole radiative-convective
350 equilibrium temperature gradient. Besides the poleward heat transport, eddies are important in
351 transporting angular momentum poleward, which maintains the easterly winds in the tropics and
352 westerlies in mid-latitudes. Similar to Fig. 7, Fig. 8a depicts the 500mb mean transient eddy heat
353 flux (black) and composite difference (green) corresponding to the weak minus strong SAMHT
354 at 20-year lead-time. Transient eddy flux is defined as $[\overline{v'T'}]$ - the product between meridional
355 wind and temperature anomalies. The primes indicate anomalies, defined by the departure of the
356 daily data from its monthly mean. Positive heat flux indicates northward flux. The anomalous
357 heat flux is about 10% of the total heat flux. The total heat flux is stronger between 45° and 60°
358 in both hemispheres. This is typically the location of the maximum momentum flux
359 convergences, and hence the location of the maximum zonal wind. The anomalous heat flux
360 (green line) is negative and equatorward (i.e., 30°) from the location of the strongest mean heat
361 flux in both hemispheres. This suggests a poleward (equatorward) shift in the NH (SH) storm
362 track or the mean location of the mid-latitude transient eddies. As a consequence, the anomalous
363 transient eddy heat flux works to cool (warm) the mid-latitudes in the NH (SH), indicating heat
364 flux divergence (convergence). That is, eddies work to reduce the anomalous temperature shown

365 in Fig. 6a. Eddy heat flux convergence must be balanced by ascending motion (red region in Fig.
366 8a). Similarly, eddy heat flux divergence must be balanced by subsidence motion (blue region in
367 Fig. 8a).

368 The zonal mean stationary eddy heat flux and composite difference are shown in Fig. 8b.
369 Stationary eddy fluxes are defined as $[\overline{v^*T^*}]$, where the stars indicate deviation from zonal mean.
370 The strongest heat flux occurs at upper levels and near the surface. The anomalous heat flux is
371 also on the order of 10% of the mean flux. Similar to the transient eddies, the anomalous heat
372 flux is in the same (opposite) direction to that of the mean stationary eddy flux in the SH (NH).
373 This suggests that stationary eddies are strengthened in the SH and weakened in the NH when
374 the SAMHT is weaker.

375 Over mid-latitudes, eddy heat flux convergence (divergence) is primarily balanced by
376 ascending (descending) motion. Similarly, momentum flux convergence (divergence) is balanced
377 by westerly (easterly) acceleration. It was shown that 20 years after the weak SAMHT, heat
378 fluxes from transient and stationary eddies converge (diverge) over the subtropical NH (SH).
379 This indicates that atmospheric eddies work in the same direction as the anomalous MMC (Fig.
380 7a) to produce anomalous ascending (descending) motion over the NH (SH) tropics, enhancing
381 the north-to-south interhemispheric heat flux. The anomalous eddy heat flux poleward of 30°N
382 (30°S) diverges (converges), producing subsidence (ascent) in the NH (SH). A more detailed
383 discussion on the SAMHT role in modifying interhemispheric atmospheric transports will be
384 presented in the discussion section.
385

386 **5. Modulation of the NH summer monsoons**

Results presented in earlier sections show that multi-decadal variation in SAMHT plays a key role in the global redistribution of heat and fresh water. It was also shown that it could provide about 15-20 years lead-time information on the atmospheric transport, including anomalous interhemispheric Hadley circulation. An important question that remains is whether such anomalous atmospheric heat and moisture transport modulates monsoonal circulation, and whether the SAMHT could be used as a potential predictor of decadal variability of the monsoons. To address this question, we will focus our attention on the NH summer monsoon season. A motivation for this question is that the NH summer climate is strongly influenced by tropical convection associated with the convectively-active monsoon phase. The monsoon is a robust component of seasonal variability. Its occurrence is highly dependent on the seasonal cycle of solar radiation, which gives rise to land-sea temperature contrast (e.g., Li and Yanai 1996; Webster et al. 1998). Beyond seasonal variations, interannual variation of the monsoon is strongly influenced by larger-scale SST anomalies linked to El Niño Southern Oscillation (ENSO) (Wang et al. 2013). Therefore, monsoon simulations require the use of coupled models that capture interaction among all climate components. Ocean-atmosphere coupling may also introduce large errors due to uncertainties in the air-sea fluxes (Bollasina and Nigam 2009), in that small errors in one component of the climate system can be exacerbated by the other components. Sperber et al. (2013) analyzed the boreal summer Asian monsoon in the Coupled Model Intercomparison Project phase 5 and 3 (i.e., CMIP5 and CMIP3) models. They found an improvement in the simulation of monsoon circulation and precipitation from CMIP3 to CMIP5 models, where the later models can reproduce some aspects (e.g., time-mean, annual cycle, intraseasonal, and interannual variability) of the monsoon.

409 Here, we will use precipitation and 850mb wind to characterize monsoon circulation in
410 CESM1. The seasonality of global precipitation is well represented by CESM1 compared to the
411 GPCC precipitation product (not shown). The largest seasonal range of precipitation is
412 concentrated on a narrow equatorial band mostly over land, e.g., South Asia, west Africa, and
413 Central America in the northern hemisphere, and Amazon basin, southeast Africa, and the
414 maritime continent in the SH. Here, monsoon regions are identified by where the June-July-
415 August-September (JJAS) minus December-January-February-March (DJFM) annual
416 precipitation range is greater than 2mm/day and the local summer precipitation exceeds 55% of
417 the total annual precipitation, following Wang et al. (2012). There are five monsoonal
418 circulations in the NH. They are the Indian (INDM), East Asian (EAM), West Pacific (WPNM),
419 North American (NAM), and North African (NAF) Monsoons. The INDM, EAM, and WPNM
420 are often studied as one monsoon circulation, referred to as the Asian summer monsoon
421 (Webster and Yang 1992). However, other studies have argued that the INDM and the EAM-
422 WPNM systems owe to two distinct convective heat sources (Goswami et al. 1999; Wang and
423 Fan 1999), where the former is forced by convection over the Arabian Sea and Bay of Bengal
424 and the latter by convection over the South China Sea and the Philippines Sea, and that these two
425 convective systems are poorly correlated. Consequently, this calls for the use of separate indices
426 to study these monsoons.

427 Before analyzing the relationship between SAMHT and the monsoons, it is necessary to
428 assess whether the model used here correctly simulates observed features of precipitation in the
429 monsoon regions. CESM1 model reproduces the mean seasonal cycle for all monsoon regions,
430 although with considerably weaker precipitation during the active phase (Fig. 9 left column).
431 Precipitation associated with the EAM is significantly weaker throughout the year when

compared to the observed. The NAM and NAF monsoons are better represented in the model compared to the other monsoons.

The lag-lead relationship of SAMHT and NH monsoons is investigated here motivated by the zonally symmetric precipitation response in the tropics (Fig. 6c). Here, Spearman rank correlation is chosen over Pearson correlation as the former is a non-parametric test that does not make assumptions on the distribution of the data. It also does not make assumption of linear relationship between each variable. These two assumptions are especially troublesome for the analysis of precipitation over monsoon regions where precipitation could be non-normally distributed and its relationship with other climate indices (e.g., SAMHT) could be non-linear. In order to test the statistical significance of Spearman rank correlation, we rely on a non-parametric test known as Kendall- τ test that measures the degree of dependence between two variables by comparing the number of concordant versus the number of discordant pairs.

Figure 9 (right-column) shows the lag-lead Spearman ranked correlation between SAMHT and NH monsoon index. The blue dashed lines depict the 95% significance level based on a non-parametric Kendall- τ test. Negative lag indicates periods when SAMHT leads the NH monsoon index. Note that the SAMHT and NH monsoon indices are significantly anticorrelated when the SAMHT leads by 15-20 years. This is consistent with result described earlier in that the atmospheric response is preceded by SAMHT by 15-20 years. This negative correlation is indicative of a strengthening of the NH monsoon precipitation when SAMHT is weak. It also suggests that SAMHT could serve as a potential predictor for decadal variability of tropical NH precipitation.

Figure 10 (left column) shows the seasonality of precipitation and 850mb winds for the INDM, EAM, NAM, and NAF monsoon regions as measured by the difference in June-July-

August-September (JJAS) minus annual mean precipitation and winds. Multidecadal variability of monsoonal circulation and precipitation is analyzed as before by the composite difference corresponding to weak minus strong SAMHT at 20-year lead-time after the anomalous SAMHT. Fig. 10 (right column) depicts the composite difference of JJAS precipitation (shaded) and 850mb rotational wind component for each monsoon region. Blue stipples indicate regions where precipitation differences are significant at 95% confidence level based on a non-parametric Kolmogorov-Smirnov test. This non-parametric test measures whether two samples (e.g., weak SAMHT period and strong SAMHT periods) have different distribution. Each region is discussed separately in bullets below:

I. Indian Monsoon (INDM, Findlater 1970; Yim et al. 2014). This monsoon circulation is associated with low-level southwesterlies and precipitation anomaly from the Arabian Sea to the Bay of Bengal (Fig. 10a). Multidecadal variability associated with weaker SAMHT is identified by enhanced precipitation over the Indian subcontinent and the Arabian Sea and less precipitation over the Indian Ocean (Fig. 10b). The circulation pattern shows enhanced southwesterly low-level jet associated with cyclonic circulation, which brings moisture convergence over India. This pattern reinforces the low-level southwesterly flow associated with the summer INDM.

II. East Asian Monsoon (EAM, Yim et al. 2014). This is a unique monsoon due to its higher latitude location. It presents itself as a dipole in precipitation (Fig. 10c). The composite difference shows a clear dipole in precipitation with positive (negative) anomaly over East China (East China Sea). Low-level anticyclonic circulation centered over southern Japan favors southwesterly flow towards east China and the Korean peninsula, bringing moisture from the Pacific Ocean. The decadal variability associated with SAMHT

478 presents a northward shift and intensification of this monsoon with respect to
479 climatology.
480 III. North American Monsoon (NAM). Although the NAM is not as robust as the other
481 monsoons mentioned above, it is an important component in seasonal precipitation over
482 northwestern Mexico and the southwestern United States (Adams and Comrie 1997;
483 Barlow et al. 1998; Cook and Seager 2013), accounting for over 70% of the annual total
484 rainfall in these regions. The composite difference shows enhanced precipitation over
485 western Mexico and the tropical eastern North Pacific Ocean (Fig. 10f). This is
486 associated with moisture flux convergence over this region and consistent with
487 strengthening of the summer monsoon (Fig. 10f).
488 IV. North African Monsoon (NAF, Yim et al. 2014). The composite difference shows
489 enhanced precipitation and low-level westerly jet, bringing moisture from the Atlantic
490 Ocean towards the Sahel region (Fig. 10h). This is consistent with the intensification of
491 the westerlies and cross-equatorial flow from the Atlantic Ocean observed during the
492 summer NAF monsoon (Fig. 10g).
493 In summary, all NH summer monsoons are enhanced during weaker a SAMHT. This is
494 consistent with enhanced south-to-north hemisphere moisture transport by the anomalous Hadley
495 circulation. Recall that there is weaker zonal flow due to anomalous southward eddy heat flux
496 over the NH north of 25°N. This creates eddy heat flux convergence and ascending motion,
497 therefore enhancing precipitation over these monsoon regions. These are important results
498 suggesting that the SAMHT is a potential source of predictability, with about 20 years lead-time,
499 of NH summer monsoon variability.
500 **6. Relative influence of the North and South Atlantic on Atmospheric Circulation**

Our analysis in previous sections indicates that decadal variability of SAMHT could modulate global atmospheric circulation and monsoons. However, since a similar link between NAMHT and global monsoons could potentially exists, it is important to understand the relative roles of SAMHT and NAMHT on modulating global monsoon variability. In other words, we need to identify whether SAMHT offers decadal predictability of global monsoons independent from that of NAMHT, which is a much more widely used index of AMOC and associated heat transport. Figure 11 depicts the anomalous interhemispheric atmospheric mass transport corresponding to a) weak minus strong SAMHT and b) weak minus strong NAMHT, similar to Fig. 5. Here, we are interested in those periods where the NAMHT and SAMHT lead the atmospheric transport (i.e., positive leads). There exists southward (i.e., negative) anomalous atmospheric heat transport about 18 years after the negative SAMHT anomaly (Fig. 11a, green line). This is also observed in the case of NAMHT, but for lead-time of about 25 years (Fig. 11b, green line).

There is difference in atmospheric response lead-times between NAMHT and SAMHT, which is depicted by diagonal magenta line in Fig. 11a and b, however, does not mean that SAMHT variability is independent from NAMHT. In fact, SAMHT variability is preceded by NAMHT variability, suggesting that the North Atlantic could provide more lead-time predictability than SAMHT. To further test, we attempted to separate the influence of the SAMHT and NAMHT on atmospheric transport by using conditional composite analysis and partial regression analysis. For this manuscript, we opt to show results from conditional composite analysis to be consistent with the rest of the paper, although both analyses give consistent results.

Figure 11c shows the annual mean (thin black) and composite difference of atmospheric

524 MMC as measured by the zonal mean 500mb atmospheric mass streamfunction. The composite
525 difference is centered at lead times according to that of Fig. 11a and b (dashed green lines). The
526 conditional composite for MMC (i.e., dependent variable) is built based on the state of the
527 SAMHT and NAMHT (i.e., independent variables). Positive (negative) values indicate
528 northward (southward) mass transport. Note that the influence of a weakening of SAMHT and
529 NAMHT onto the MMC has similar amplitude. Also, the amplitude of the MMC anomaly is
530 larger when both MHT indices are considered. This suggests that both the SAMHT and NAMHT
531 and associated HC anomalies influence atmospheric circulation and transport. Although, the
532 NAMHT leads the SAMHT negative HC anomaly in the South Atlantic associated with SAMHT
533 divergence works in par with positive HC anomaly in the North Atlantic due to NAMHT
534 convergence (see Fig. 4b), creating an interhemispheric asymmetry in energy balance. This
535 asymmetry drives an anomalous Hadley circulation which transport heat from the NH to the SH
536 (Fig. 11c green contour).

537 Several studies have suggested that the North Atlantic Oscillator (NAO) is a precursor of
538 NAMHT variability, through wind stress and heat flux forcing in the high-latitudes oceanic
539 convection regions (e.g., Eden and Willebrand 2001, Medhaug et al. 2012, Sun et al. 2015).
540 Here, we address the relationship of NAMHT and SAMHT with the NAO. Fig. 12a show the
541 lag-lead composite difference of NAO index for weak minus strong SAMHT (red) and NAMHT
542 (blue). As suggested in Sun et al. (2015), the negative phase of the NAO precedes the weakening
543 of NAMHT by about 15 years. This delayed effect is due to large inertia associated with slow
544 oceanic processes. The reduced AMOC and NAMHT have a negative feedback in that the NAO
545 shows a delayed response (i.e., positive phase) about 18 years after the weakening of the

546 NAMHT. However, the relationship between SAMHT and NAO is not robust. Thus, NAO does
547 not give a predictability of SAMHT.
548
549 **7. Summary and Discussion**
550 This study tested the hypothesis whether low frequency (decadal) variability of the South
551 Atlantic MOC and MHT influence decadal variability of climate events over the globe. A multi-
552 century climate simulation based on a state-of-the-art coupled GCM was used as the basis for our
553 analysis. Multi-decadal variability of the South Atlantic Ocean has been shown to play a key role
554 in modulating atmospheric dynamics including the distribution of momentum, heat, and fresh
555 water. For this reason, it is of great importance to the climate community to understand the role
556 that the ocean plays and the physical mechanism behind this hypothesis. In this section, we
557 highlight this mechanism, which was described in previous sections, using two summary
558 schematic diagrams presented in Figs. 13 and 14.
559 The first diagram (Fig. 13) shows the transient evolution of MHT anomaly over the
560 tropical Atlantic Ocean during weak minus strong SAMHT. Here, the gray shading indicates the
561 anomalous negative MHT (i.e., weakening of the northward heat transport). The anomaly
562 propagates from north-to-south (black arrows), where the anomaly at 30°N leads the anomaly at
563 30°S by about 10-12 years with an approximate speed of ~600km/year. The largest amplitudes
564 occur away from the equator. When the maximum anomaly arrives at 30°S (i.e., the location of
565 our composite SAMHT or 0-year lag), there is MHT divergence between 30°S and the equator,
566 highlighted by the dark-blue hatching and easily identified by the increased MHT southward
567 away from the equator. The MHT divergence is balanced by negative heat content tendency,
568 which results in negative heat content anomaly over the South Atlantic and negative SST

anomaly about 15-20 years later, shown by blue shading. The positive heat content anomaly in the NH is mostly due to MHT convergence approximately 10-12 years earlier. This creates an interhemispheric HC anomaly. The impact of these heat content anomalies on atmospheric circulation is discussed next.

The diagram in Fig. 14 shows the zonal mean atmospheric (top) and Atlantic Ocean (bottom) circulation. As discussed with respect to Fig. 13, weaker MHT (thick arrows on bottom panel) is associated with negative tendency in heat content over the subtropical South Atlantic (blue stipples at 0-year lag in Fig. 13). The heat content tendency is dominated by meridional MHT divergence (blue stipples in Fig. 13), producing a negative heat content anomaly approximately 15-20 years later. The negative (positive) heat content anomaly in the SH (NH) forces subsidence and anomalous Hadley circulation (gray oval and counterclockwise circulation in Fig. 14) that brings moisture from the SH to the NH (green arrow) and heat from the NH towards the SH (purple arrow). This anomalous interhemispheric atmospheric circulation is supported by a net gain in radiative fluxes at the top of the atmosphere (labeled R_{TOA}) over the NH and net radiative loss over the SH represented by red and blue arrows, respectively. In addition, there is a net positive surface heat flux downward in the SH (blue arrows labeled heat flux). Atmospheric eddies, both transient and stationary, transport heat southward in both hemispheres (purple arrows) to balance the radiative fluxes. This produces eddy heat flux convergence around 15°N and divergence around 15°S (stipples), reinforcing the anomalous Hadley circulation. Poleward of 30° latitude, anomalous atmospheric eddies produce heat flux divergence (convergence) in the NH (SH), which causes sinking (rising) motion. This is consistent with a poleward (equatorward) displacement of the jet stream and mean storm track and enhanced (reduced) TOA radiation in the NH (SH). The poleward (equatorward)

592 displacement of the jet stream is a consequence of thermal wind balance from a reduced
593 (enhanced) meridional temperature gradient over NH (SH) mid-latitudes. The poleward
594 (equatorward) shift of the mean zonal jet in the NH (SH) causes eddy momentum flux
595 convergence (divergence). This must be balanced by poleward (equatorward) flow at upper
596 levels. This flow pattern supports a thermally indirect eddy driven circulation in both
597 hemispheres (circulation labeled eddies in Fig. 14). This circulation brings anomalous ascent and
598 more precipitation from 15°N-30°N, and descent and less precipitation poleward of 30°N. The
599 opposite occurs in the SH, with descent and less precipitation from 30°S-15°S and ascent
600 poleward of 30°S. In summary, the NH atmosphere behaves like the summer hemisphere,
601 conversely, the SH behaves like the winter hemisphere, approximately 15-20 years after the
602 anomalous negative SAMHT.

603 The proposed mechanism is in contrast with that of Sun et al. (2015) which suggests that
604 the North Atlantic MOC can influence the SH mid-latitude zonal wind and precipitation. They
605 found that strengthening of the North Atlantic MOC induces a subpolar interhemispheric SST
606 seesaw pattern, with cold SST anomalies in high latitudes Southern Ocean. This leads to an
607 enhanced meridional temperature gradient, increasing the zonal winds. The associated changes in
608 the zonal wind could potentially influence SAMHT, explaining the lead-lag relationship of
609 NAMHT and SAMHT. Although, we found that the geostrophic component of the SAMHT
610 explains most of the low-frequency variance of the total SAMHT, whereas the Ekman (i.e.,
611 wind-forced) component is comprised of higher frequencies. Further investigations on the
612 contrasting mechanisms are necessary but beyond the scope of this study.

613

614 **8. Conclusion**

615 This is the first attempt to link the South Atlantic Overturning Circulation variability to
616 weather and climate. The anomalous circulation pattern associated with SAMHT variability
617 discussed throughout this paper has great implications for long-term climate variability over the
618 whole globe. For example, it could bring drier and warmer summer conditions over North
619 America and Europe. The results presented here suggest the possibility of decadal predictability
620 of seasonal temperature and precipitation, more so for those regions affected by monsoonal
621 circulation. It was shown that decadal modulation of the NH summer monsoon is tied to
622 variability of the SAMHT. Intensification of the NH summer monsoon is through a northward
623 shift and strengthening of the ITCZ when the SAMHT is weak via upper ocean heat content
624 modification. This proposed mechanism utilizing the atmospheric energy budget to understand
625 the ITCZ location is consistent with Kang et al. (2009) and Broccoli et al. (2006). Our hypothesis
626 of a tropical control of the location of the ITCZ is in contrast with the possibility of a high-
627 latitude control of the ITCZ location proposed in Frierson et al. (2013). The ITCZ in this study is
628 shifted towards the warmer hemisphere, which is the NH, about 15-20 years after a weakening of
629 the SAMHT.

630 The main objective here was to highlight the important role of the SAMHT in modifying
631 atmospheric circulation. Most of the current literature places their effort in the North Atlantic.
632 Here, we showed that the South Atlantic variability offers potential for added predictability of
633 the climate system. Our argument that the SAMHT could modify the strength and location of the
634 ITCZ has important implications, because the slowly-varying South Atlantic circulation could
635 serve as potential predictor for decadal variability of the global monsoon system giving a lead-
636 time of about 15-20 years from the anomalous MHT to its climate effects. Being this one of the
637 first studies that investigates the role of the South Atlantic on climate and monsoons, further

638 efforts are necessary to confirm these results. For example, the processes that are responsible
639 for the SAMHT variability are unclear. Is the SAMHT only a consequence of North Atlantic
640 variability, or is it driven by independent local processes in the South Atlantic such as those
641 mentioned in introduction? The relative roles of the North and South Atlantic MOC on the
642 climate system needs further investigation. In future works, special emphasis will be given to
643 high impact extreme weather events, such as droughts and heat waves. Also, the relative role of
644 internal climate variability, like SAMHT, versus external forcing is an important question given
645 the current climate projections (e.g., Lee et al. 2014). Results presented here highlight the need
646 for continuous improvements in coupled models as well as the value of sustained ocean
647 observational efforts, both necessary to improve our knowledge of the complex interaction
648 between the South Atlantic MOC and global climate variability.
649
650 *Acknowledgement:* This research was carried out in part under the auspices of the Cooperative
651 Institute of Marine and Atmospheric Studies, a cooperative institute of the University of Miami
652 and the National Oceanic and Atmospheric Administration (NOAA), cooperative agreement
653 NA10OAR4320143. This work was supported by NOAA Atlantic Oceanographic and
654 Meteorological Laboratory and funded by Climate Observations Division of the Climate
655 Program Office.
656
657 **Reference**
658 Adams, D. K., and A. C. Comrie (1997), The north American monsoon, *Bulletin of the American*
659 *Meteorological Society*, *78*(10), 2197-2213.

660 Ambrizzi, T., B. J. Hoskins, and H.-H. Hsu (1995), Rossby wave propagation and teleconnection
661 patterns in the austral winter, *Journal of the Atmospheric Sciences*, *52*(21), 3661-3672.
662 Barlow, M., S. Nigam, and E. H. Berbery (1998), Evolution of the North American monsoon
663 system, *Journal of Climate*, *11*(9), 2238-2257.
664 Becker, A., P. Finger, A. Meyer-Christoffer, B. Rudolf, K. Schamm, U. Schneider, and M. Ziese
665 (2013), A description of the global land-surface precipitation data products of the Global
666 Precipitation Climatology Centre with sample applications including centennial (trend)
667 analysis from 1901-present, *Earth System Science Data*, *5*, 71-99.
668 Biastoch, A., C. W. Böning, F. U. Schwarzkopf, and J. Lutjeharms (2009), Increase in Agulhas
669 leakage due to poleward shift of Southern Hemisphere westerlies, *Nature*, *462*(7272),
670 495-498.
671 Bollasina, M., and S. Nigam (2009), Indian Ocean SST, evaporation, and precipitation during the
672 South Asian summer monsoon in IPCC-AR4 coupled simulations, *Clim Dyn*, *33*(7-8),
673 1017-1032.
674 Broccoli, A. J., K. A. Dahl, and R. J. Stouffer, 2006: Response of the ITCZ to Northern
675 Hemisphere cooling. Geophys. Res. Lett., 33, L01702, doi:10.1029/2005GL024546.
676 Broecker, W. S. (1991), The great ocean conveyor, *Oceanography*, *4*(2), 79-89.
677 Broecker, W. S., Peteet, D. M. & Rind, D (1985). Does the ocean-atmosphere system have more
678 than one stable mode of operation? *Nature* **315**, 21–26
679 Cassou, C., L. Terray, and A. S. Phillips (2005), Tropical Atlantic influence on European heat
680 waves, *Journal of climate*, *18*(15), 2805-2811.

681 Cassou, C., C. Deser, L. Terray, J. W. Hurrell, and M. Drévillon (2004), Summer sea surface
682 temperature conditions in the North Atlantic and their impact upon the atmospheric
683 circulation in early winter, *Journal of climate*, *17*(17), 3349-3363.
684 Chiang, J. C., and C. M. Bitz (2005), Influence of high latitude ice cover on the marine
685 Intertropical Convergence Zone, *Clim Dyn*, *25*(5), 477-496.
686 Clark, P. U., Pisias, N. G., Stocker, T. F. & Weaver, A. J. (2002). The role of the thermohaline
687 circulation in abrupt climate change. *Nature* **415**, 863–869.
688 Cook, B., and R. Seager (2013), The response of the North American Monsoon to increased
689 greenhouse gas forcing, *Journal of Geophysical Research: Atmospheres*, *118*(4), 1690-
690 1699.
691 Corti, S., A. Weisheimer, T. Palmer, F. Doblas-Reyes, and L. Magnusson (2012), Reliability of
692 decadal predictions, *Geophysical Research Letters*, *39*(21).
693 Cunningham, S. A., T. Kanzow, D. Rayner, M. O. Baringer, W. E. Johns, J. Marotzke, H. R.
694 Longworth, E. M. Grant, J. J.-M. Hirschi, and L. M. Beal (2007), Temporal variability of
695 the Atlantic meridional overturning circulation at 26.5 N, *science*, *317*(5840), 935-938.
696 Danabasoglu, G., and J. Marshall (2007), Effects of vertical variations of thickness diffusivity in
697 an ocean general circulation model, *Ocean Modelling*, *18*(2), 122-141.
698 Danabasoglu, G., S. C. Bates, B. P. Briegleb, S. R. Jayne, M. Jochum, W. G. Large, S. Peacock,
699 and S. G. Yeager (2012), The CCSM4 ocean component, *Journal of Climate*, *25*(5),
700 1361-1389.
701 Drévillon, M., L. Terray, P. Rogel, and C. Cassou (2001), Mid latitude Atlantic SST influence on
702 European winter climate variability in the NCEP reanalysis, *Clim Dyn*, *18*(3-4), 331-344.

703 Dong, S. S. L. Garzoli, M. O. Baringer, C. S. Meinen, and G. J. Goni, 2009: Interannual
704 variations in the Atlantic meridional overturning circulation and its relationship with the
705 net northward heat transport in the South Atlantic. Geophys. Res. Lett., 36, L20606,
706 doi:10.1029/2009GL039356
707 Dong, S., M. Baringer, G. Goni, and S. Garzoli, 2011: Importance of the assimilation of Argo
708 Float Measurements on the Meridional Overturning Circulation in the South Atlantic.
709 Geophys. Res. Lett., 38, L18603, doi:10.1029/2011GL048982.
710 Dong, S., S.L. Garzoli, and M.O. Baringer, 2011: The role of inter-ocean exchanges on decadal
711 variations of the northward heat transport in the South Atlantic. J. Phys. Oceanogr.,
712 41(8):1498-1511.
713 Dong, S. , M. O. Baringer , G. J. Goni , C. S. Meinen , and S. L. Garzoli, 2014: Seasonal
714 variations in the South Atlantic Meridional Overturning Circulation from observations
715 and numerical models , Geophys. Res. Lett ., 41 , 4611 - 4618 , doi:
716 10.1002/2014GL060428.
717 Dong, S ., G. Goni , and F. Bringas , 2015: Temporal variability of the Meridional Overturning
718 Circulation in the South Atlantic between 20°S and 35°S, *Geophys. Res. Lett.*,
719 doi:10.1002/2015GL065603.
720 Eden C. and J. Willebrand (2001), Mechanism of interannual to decadal variability of the
721 North Atlantic Circulation. J. Climate, 14, 2266-2280.
722 Enfield, D. B., A. M. Mestas-Nuñez, and P. J. Trimble (2001), The Atlantic multidecadal
723 oscillation and its relation to rainfall and river flows in the continental US, *Geophysical*
724 *Research Letters*, *28*(10), 2077-2080.

725 Ferrari, R., J. C. McWilliams, V. M. Canuto, and M. Dubovikov (2008), Parameterization of
726 eddy fluxes near oceanic boundaries, *Journal of Climate*, *21*(12), 2770-2789.
727 Findlater, J. (1970), A major low-level air current near the Indian Ocean during the northern
728 summer, *Quarterly Journal of the Royal Meteorological Society*, *95*(404), 362-380.
729 Frierson, D. M., Y.-T. Hwang, N. S. Fučkar, R. Seager, S. M. Kang, A. Donohoe, E. A. Maroon,
730 X. Liu, and D. S. Battisti (2013), Contribution of ocean overturning circulation to tropical
731 rainfall peak in the Northern Hemisphere, *Nature Geoscience*, *6*(11), 940-944.
732 Garzoli, S. L., and Z. Garraffo (1989), Transports, frontal motions and eddies at the Brazil-
733 Malvinas Currents Confluence, *Deep Sea Research Part A. Oceanographic Research*
734 *Papers*, *36*(5), 681-703.
735 Garzoli, S. L., and R. Matano (2011), The South Atlantic and the Atlantic meridional overturning
736 circulation, *Deep Sea Research Part II: Topical Studies in Oceanography*, *58*(17), 1837-
737 1847.
738 Goni, G.J., F. Bringas, and P.N. Di Nezio, (2011), Observed Low Frequency Variability of the
739 Brazil Current Front. *J. Geophys. Res.,* 116, C10037, doi:10.1029/2011JC007198.
740 Gordon, A. L. (1985), Indian-Atlantic transfer of thermocline water at the Agulhas Retroflection,
741 *Science*, *227*(4690), 1030-1033.
742 Goswami, B. N., V. Krishnamurthy, and H. Annmalai (1999), A broad-scale circulation index for
743 the interannual variability of the Indian summer monsoon, *Quarterly Journal of the Royal*
744 *Meteorological Society*, *125*(554), 611-633.
745 Hawkins, E. *et al.* (2011). Bistability of the Atlantic overturning circulation in a global climate
746 model and links to ocean freshwater transport. *GRL* **38**, L10605.

747 Jochum, M. (2009), Impact of latitudinal variations in vertical diffusivity on climate simulations,
748 *Journal of Geophysical Research: Oceans (1978–2012)*, *114*(C1).
749 Jochum, M., G. Danabasoglu, M. Holland, Y. O. Kwon, and W. Large (2008), Ocean viscosity
750 and climate, *Journal of Geophysical Research: Oceans (1978–2012)*, *113*(C6).
751 Johns, W. E., M. O. Baringer, L. Beal, S. Cunningham, T. Kanzow, H. L. Bryden, J. Hirschi, J.
752 Marotzke, C. Meinen, and B. Shaw (2011), Continuous, array-based estimates of Atlantic
753 Ocean heat transport at 26.5 N, *Journal of Climate*, *24*(10), 2429-2449.
754 Kang, S. M., D. M. Frierson, and I. M. Held (2009), The tropical response to extratropical
755 thermal forcing in an idealized GCM: The importance of radiative feedbacks and
756 convective parameterization, *Journal of the atmospheric sciences*, *66*(9), 2812-2827.
757 Kang, S. M., I. M. Held, and S.-P. Xie, (2014), Contrasting the tropical response to zonally
758 asymmetric extratropical and tropical forcing, *Clim Dyn*., **42,** (2033-2043).
759 Kay, J., C. Deser, A. Phillips, A. Mai, C. Hannay, G. Strand, J. Arblaster, S. Bates, G.
760 Danabasoglu, and J. Edwards (2014), The Community Earth System Model (CESM)
761 Large Ensemble Project: A community resource for studying climate change in the
762 presence of internal climate variability, *Bulletin of the American Meteorological Society*.
763 Klinger, B. A., and J. Marotzke (2000), Meridional heat transport by the subtropical cell, *Journal*
764 *of physical oceanography*, *30*(4), 696-705.
765 Knight, J. R., R. J. Allan, C. K. Folland, M. Vellinga, and M. E. Mann (2005), A signature of
766 persistent natural thermohaline circulation cycles in observed climate, Geophys. Res.
767 Lett., 32, L20708, doi:10.1029/2005GL024233.
768 Knight, J. R , C. K. Folland, and A. A. Scaife (2006), Climate impacts of the Atlantic
769 multidecadal oscillation. Geophys. Res. Lett., 33,L17706, doi:10.1029/2006GL026242.

770 Kriegler, E., Hall, J. W., Held, H., Dawson, R. & Schellnhuber, H. J. (2009). Imprecise
771 probability assessment of tipping points in the climate system. *PNAS* **106**, 5041–5046.
772 Las Heras, M. M., and R. Schlitzer (1999), On the importance of intermediate water flows for the
773 global ocean overturning, *Journal of Geophysical Research: Oceans (1978–2012)*,
774 *104*(C7), 15515-15536.
775 Latif, M., K. Arpe, and E. Roeckner (2000), Oceanic control of decadal North Atlantic sea level
776 pressure variability in winter, *Geophysical Research Letters*, *27*(5), 727-730.
777 Latif, M., M. Collins, H. Pohlmann, and N. Keenlyside (2006), A review of predictability studies
778 of Atlantic sector climate on decadal time scales, *Journal of Climate*, *19*(23), 5971-5987.
779 Latif, M., E. Roeckner, M. Botzet, M. Esch, H. Haak, S. Hagemann, J. Jungclaus, S. Legutke, S.
780 Marsland, and U. Mikolajewicz (2004), Reconstructing, monitoring, and predicting
781 multidecadal-scale changes in the North Atlantic thermohaline circulation with sea
782 surface temperature, *Journal of Climate*, *17*(7), 1605-1614.
783 Lee, J.-Y., B. Wang, K.-H. Seo, J.-S. Kug, Y.-S. Choi, Y. Kosaka, and K.-J. Ha, 2014: Future
784 Change of Northern Hemisphere Summer Tropical–Extratropical Teleconnection in
785 CMIP5 Models. J. Climate, 27, 3643–3664. doi: http://dx.doi.org/10.1175/JCLI-D-13-
786 00261.1
787 Lee, S.-K. and C. Wang (2010), Delayed advective oscillation of the Atlantic thermohaline
788 circulation. *J. Climate*, **23**, 1254-1261.
789 Lee, S. K., W. Park, E. van Sebille, M. O. Baringer, C. Wang, D. B. Enfield, S. G. Yeager, and
790 B. P. Kirtman (2011), What caused the significant increase in Atlantic Ocean heat content
791 since the mid-20th century?, *Geophysical Research Letters*, *38*(17).

792 Lee, S.-K., C. R. Mechoso, C. Wang and J. D. Neelin (2013), Interhemispheric influence of the
793 northern summer monsoons on the southern subtropical anticyclones. *J. Climate*, **26**,
794 10193-10204, doi:http://dx.doi.org/10.1175/JCLI-D-13-00106.1.
795 Lenton, T. M. *et al.* (2009). Using GENIE to study a tipping point in the climate system. *Phil.*
796 *Trans. A* **367**, 871–884.
797 Li, C., and M. Yanai (1996), The onset and interannual variability of the Asian summer monsoon
798 in relation to land-sea thermal contrast, *Journal of Climate*, *9*(2), 358-375.
799 Lumpkin, R., and K. Speer (2007), Global ocean meridional overturning, *Journal of Physical*
800 *Oceanography*, *37*(10), 2550-2562.
801 Manabe, S. & Stouffer, R. J. (1988). Two stable equilibria of a coupled ocean-atmosphere
802 model. *J. Climate* **1**, 841–866.
803 McPhaden, M. J., and D. Zhang (2002), Slowdown of the meridional overturning circulation in
804 the upper Pacific Ocean, *Nature*, *415*(6872), 603-608.
805 McPhaden, M. J., and D. Zhang (2004), Pacific Ocean circulation rebounds, *Geophysical*
806 *Research Letters*, *31*(18).
807 Medhaug I., H. R. Langehaug, T. Eldevik, T. Furevik and M. Bentsen (2012) Mechanisms for
808 decadal scale variability in a simulated Atlantic meridional overturning circulation.
809 Clim. Dyn., 39, 77-93.
810 Nairn, J., R. Fawcett, and D. Ray (2009), Defining and predicting Excessive Heat events, a
811 National system, paper presented at Proceedings of the CAWCR modelling workshop:
812 understanding high impact weather, Citeseer.
813 Neale, R. B., J. H. Richter, and M. Jochum (2008), The impact of convection on ENSO: From a
814 delayed oscillator to a series of events, *Journal of climate*, *21*(22), 5904-5924.

Peings, Y. and G. Magnusdottir (2014), Forcing of the wintertime atmospheric circulation by the multidecadal fluctuations of the North Atlantic ocean, Environ. Res. Lett. 9 034018 doi:10.1088/1748-9326/9/3/034018.

Rahmstorf, S. *et al.* (2005). Thermohaline circulation hysteresis: A model intercomparison. *Geophys. Res. Lett.* **32**, L23605.

Rodwell, M. J., and C. K. Folland (2003), Atlantic air-sea interaction and model validation, *Annals of Geophysics*.

Saunders, P. M., and B. A. King (1995), Oceanic fluxes on the WOCE A11 section, *Journal of Physical Oceanography*, *25*(9), 1942-1958.

Sloyan, B. M., and S. R. Rintoul (2001), The southern ocean limb of the global deep overturning circulation, *Journal of Physical Oceanography*, *31*(1), 143-173.

Sperber, K. R., H. Annamalai, I.-S. Kang, A. Kitoh, A. Moise, A. Turner, B. Wang, and T. Zhou (2013), The Asian summer monsoon: an intercomparison of CMIP5 vs. CMIP3 simulations of the late 20th century, *Clim Dyn*, *41*(9-10), 2711-2744.

Stommel, H. (1961). Thermohaline convection with two stable regimes of flow. *Tellus* **13**, 224–230.

Stouffer, R. J., J. Yin, J. Gregory, K. Dixon, M. Spelman, W. Hurlin, A. Weaver, M. Eby, G. Flato, and H. Hasumi (2006), Investigating the causes of the response of the thermohaline circulation to past and future climate changes, *Journal of Climate*, *19*(8), 1365-1387.

Sun, C., J. Li, F. F. Jin, and R. Q. Ding, 2013: Sea surface temperature inter-hemispheric dipole and its relation to tropical precipitation. Environ. Res. Lett., 8, doi:10.1088/1748-9326/8/4/044006

837 Sun, C., J. Li, and F.-F. Jin (2015), A delayed oscillator model for the quasi-periodic
838 multidecadal variability of the NAO, *Clim Dyn*, 1-17.
839 Sun, C., J. Li, J. Feng, F. Xie, 2015: A Decadal-Scale Teleconnection between the North
840 Atlantic Oscillation and Subtropical Eastern Australian Rainfall. Journal of Climate,
841 28, 1074-1092
842 Sutton, R. T., and D. L. Hodson (2005), Atlantic Ocean forcing of North American and European
843 summer climate, *Science*, *309*(5731), 115-118.
844 Talley, L. D. (2003), Shallow, intermediate, and deep overturning components of the global heat
845 budget, *Journal of Physical Oceanography*, *33*(3), 530-560.
846 Ting, M., Y. Kushnir, R. Seager, and C. Li (2011), Robust features of Atlantic multi-decadal
847 variability and its climate impacts, Geophys. Res. Lett., 38, L17705,
848 doi:10.1029/2011GL048712.
849 Trenberth, K. E., and J. M. Caron (2001), Estimates of meridional atmosphere and ocean heat
850 transports, *Journal of Climate*, *14*(16), 3433-3443.
851 Tung, K.-K., and J. Zhou (2013), Using data to attribute episodes of warming and cooling in
852 instrumental records, *Proceedings of the National Academy of Sciences*, *110*(6), 2058-
853 2063.
854 Wang, B., and Z. Fan (1999), Choice of South Asian summer monsoon indices, *Bulletin of the*
855 *American Meteorological Society*, *80*(4), 629-638.
856 Wang, B., R. Wu, and K. Lau (2001), Interannual variability of the Asian summer monsoon:
857 contrasts between the Indian and the Western North Pacific-East Asian Monsoons*,
858 *Journal of Climate*, *14*(20), 4073-4090.
859 Wang H, Wang B, Huang F, Ding Q, Lee JY (2012) Interdecadal change of the boreal summer

860 circumglobal teleconnection (1958–2010). Geophys Res Lett 39:L12704

861 Wang, B., J. Liu, H.-J. Kim, P. J. Webster, S.-Y. Yim, and B. Xiang (2013), Northern
862 Hemisphere summer monsoon intensified by mega-El Niño/southern oscillation and
863 Atlantic multidecadal oscillation, *Proceedings of the National Academy of Sciences*,
864 *110*(14), 5347-5352.

865 Webster, P. J., and S. Yang (1992), Monsoon and ENSO: Selectively interactive systems,
866 *Quarterly Journal of the Royal Meteorological Society*, *118*(507), 877-926.

867 Webster, P. J., V. O. Magana, T. Palmer, J. Shukla, R. Tomas, M. u. Yanai, and T. Yasunari
868 (1998), Monsoons: Processes, predictability, and the prospects for prediction, *Journal of*
869 *Geophysical Research: Oceans (1978–2012)*, *103*(C7), 14451-14510.

870 Weijer, W., B. M. Sloyan, M. E. Maltrud, N. Jeffery, M. W. Hecht, C. A. Hartin, E. van Sebille,
871 I. Wainer, and L. Landrum (2012), The Southern Ocean and its climate in CCSM4,
872 *Journal of Climate*, *25*(8), 2652-2675.

873 Yim, S. Y., Wang, B., Liu, J., & Wu, Z. (2014), A comparison of regional monsoon variability
874 using monsoon indices. *Climate Dynamics*, *43*(5-6), 1423-1437.

875 Yoshimori, M., and A. J. Broccoli (2008), Equilibrium response of an atmosphere-mixed layer
876 ocean model to different radiative forcing agents: Global and zonal mean response,
877 *Journal of Climate*, *21*(17), 4399-4423.

878 Zhang, L., and C. Wang (2013), Multidecadal North Atlantic sea surface temperature and
879 Atlantic meridional overturning circulation variability in CMIP5 historical simulations,
880 *Journal of Geophysical Research: Oceans*, *118*(10), 5772-5791.

881 Zhang, R., and T. L. Delworth (2005), Simulated tropical response to a substantial weakening of
882 the Atlantic thermohaline circulation, *Journal of Climate*, *18*(12), 1853-1860.

Zhang, R., and T. L. Delworth (2006), Impact of Atlantic multidecadal oscillations on India/Sahel rainfall and Atlantic hurricanes. Geophys. Res. Lett., 33, L17712, doi:10.1029/2006GL026267.Zickfeld, K. *et al.* (2007). Expert judgments on the response of the Atlantic Meridional Overturning Circulation to climate change. *Climatic Change* **82**, 235–265.

Figure captions

Figure 1. Meridional heat transport over the Atlantic Ocean (PetaWatts) from CESM1 model (black), gray shading represents one standard deviation. Also shown are estimated transports from NCEP (blue) and ECMWF reanalysis (red) from Trenberth et al. (2001). Direct estimates from the RAPID array at 26°N are shown in brown. Transport estimates from ARGO, XBTs, and altimetry observations at 34°S are shown by green color. The color shading and vertical bars depict one standard deviation calculated from annual average of MHT for each latitude.

Figure 2. 11-year running average of the SAMHT timeseries for a) total, b) Ekman, and c) geostrophic component for the 1100 model year analyzed. The total timeseries is defined as the meridional heat transport at 30°S after removing the seasonal cycle and linear trend. The Ekman component is estimated using monthly mean zonal wind stress from CESM1, whereas the geostrophic term is simply taken as the difference between the total and Ekman component. The red (blue) line fill contours indicate values greater (less) than one standard deviation.

Figure 3. The mean ocean meridional overturning streamfunction for the Atlantic (top) and global ocean (bottom), where positive streamfunction indicates clockwise flow. The mean

906 circulation is taken as the time mean, whereas the anomalous circulation is defined by the
907 composite difference between weak minus strong SAMHT, shown by color shading.

908 Figure 4. a) Lead-lag composite difference of zonal mean Atlantic MHT with respect to weak
909 minus strong SAMHT. b), c), d) and e) are similar to a) but for 700m Atlantic Ocean heat
910 content (HC), heat content tendency, MHT divergence (positive for convergence), and net
911 surface energy flux (positive downward into the ocean) respectively. Color shading indicates
912 95% significance using a Kendall-tau test. The y-axis indicates time in years. Time progresses up
913 the page with lag (lead) indicating SAMHT lags (leads), respectively.

914 Figure 5. Lead-lag composite difference of interhemispheric atmospheric circulation depicted as
915 the vertically integrated mass transport about the equator for weak minus strong SAMHT. Here,
916 the direction of interhemispheric atmospheric heat transport is proportional to the mass transport
917 with northward (southward) labeled red (blue). Color shading indicates 95% significance using a
918 student-T test. The y-axis indicates time in years. Time progresses up the page with lag (lead)
919 indicating that SAMHT lags (leads), respectively.

920 Figure 6. Composite difference of a) 500mb air temperature, b) sea surface temperature, and c)
921 precipitation corresponding to weak minus strong SAMHT at 20-year lead-time (i.e., 20 years
922 after the anomalous SAMHT.

923 Figure 7. a) Time mean and zonal mean meridional circulation (MMC) of the atmosphere as
924 measured by the mass streamfunction (contour) and composite difference (color) with respect to
925 weak minus strong SAMHT at 20-year lead time (i.e., 20 years after the anomalous SAMHT, see
926 Fig. 4). Panels b) and c) are similar to a) but for the meridional heat flux b), and meridional

927 moisture flux c), respectively. Mean northward heat and moisture flux are indicated by positive
928 contours and positive shading depicts anomalous northward fluxes.

929 Figure 8. a) 500mb mean transient eddy heat flux (black) and composite difference (green)
930 during weak minus strong SAMHT. Anomalous heat flux convergence (divergence) is
931 highlighted by red (blue) regions on the composite difference line. b) Stationary eddy heat flux
932 (black contour) and composite difference (color shading) during weak minus strong SAMHT.
933 Similar to Fig. 7, the composite difference is analyzed 20 years after the anomalous SAMHT.

934 Figure 9. (left column) Seasonality of precipitation of the four monsoon regions (i.e., Indian
935 (INDM), East Asian (EAM), North American (NAM), and North African Monsoon (NAF)) from
936 GPCC (blue) and CESM1 (red). Error bars indicate the 99% confidence level. (right-column)
937 Lag-lead Spearman ranked correlation between SAMHT and NH monsoon index. The blue
938 dashed lines depict the 95% significance level based on a non-parametric Kendall-τ test.
939 Negative lag indicates periods when SAMHT leads the NH monsoon index. Periods with
940 significant correlation are shaded blue.

941 Figure 10. (left column) Seasonality of precipitation and 850mb winds for the monsoon regions
942 (i.e., Indian (INDM), East Asian (EAM), North American (NAM), and North African Monsoon
943 (NAF) as measured by the difference between June-July-August-September (JJAS) minus annual
944 mean precipitation and winds. (right-column) The composite difference of JJAS precipitation
945 (shaded) and 850mb wind for each monsoon region with respect to weak minus strong SAMHT
946 at lead-time 20 years after the anomalous SAMHT. Blue stipples indicates regions where
947 precipitation differences are significant at 95% confidence level based on a non-parametric
948 Kolmogorov-Smirnov test.

949 Figure 11. Anomalous interhemispheric atmospheric mass transport corresponding to a) weak
950 minus strong SAMHT and b) weak minus strong NAMHT, similar to Fig. 5. The diagonal
951 magenta line between panels a) and b) highlights the fact that NAMHT leads SAMHT. c) Annual
952 mean (thin black) and composite difference of atmospheric mean meridional circulation (MMC)
953 as measured by the zonal mean 500mb atmospheric mass streamfunction. The composite
954 difference is centered at lead times according to that of a) and b) (dashed green lines). The
955 conditional composite for MMC (i.e., dependent variable) is built based on the state of the
956 SAMHT and NAMHT (i.e., independent variables). The green contour here includes the
957 relationship between the MMC with both, SAMHT and NAMHT. Red contour depicts the
958 relationship between NAMHT and the MMC excluding the influence of SAMHT (i.e., neutral
959 SAMHT periods based on terciles). Similarly, blue contour shows the relationship between
960 SAMHT and the MMC excluding the influence of NAMHT (i.e., neutral NAMHT periods based
961 on terciles). Positive (negative) values indicate northward (southward) mass transport.

962 Figure 12. a) Lead-lag composite difference of North Atlantic Oscillator (NAO) index for weak
963 minus strong SAMHT (red) and weak minus strong NAMHT (blue). The y-axis indicates time in
964 years. Time progresses up the page with lag (lead) indicating the ocean MHT lags (leads),
965 respectively. b) 500mb geopotential height anomaly associated with the positive phase of the
966 NAO.

967 Figure 13. **Transient evolution of MHT anomaly over the tropical Atlantic Ocean during**
968 **weak minus strong SAMHT.** Gray shading indicates the anomalous negative MHT (i.e.,
969 weakening of the northward heat transport). The anomaly propagates from north to south (black
970 arrows) at about 600km/year. The dark-red hatched region indicates meridional heat transport
971 convergence and positive heat content tendency north of the equator 10-15 years prior to the

weak minus strong SAMHT, whereas the dark-blue hatched region indicates meridional heat transport divergence and negative heat content tendency south of the equator near 0-lag with respect to weak minus strong SAMHT. Blue (red) shading depicts negative (positive) heat content. The y-axis indicates time in years. Time progresses up the page, with lag (lead) indicating SAMHT lags (leads), respectively. Anomalous heat content occurs about 15-20 years after the anomalous heat content tendency and heat transport divergence in both hemispheres.

Figure 14. **Schematic diagram of the role of weaker-than-normal MHT in the anomalous atmospheric circulation at 15-20 years lead-time.** Weakened MHT is shown by thick black arrows on the bottom panel. Negative (positive) tendency in heat content is labeled by dark-blue (red) hatching. There is negative (positive) heat content in the SH (NH) about 15-20 years after the heat transport anomaly labeled here by blue (red) rectangle. Anomalous Hadley circulation is labeled by gray oval and counterclockwise circulation. Moisture and heat fluxes are shown by green and purple arrows, respectively. The TOA and surface radiative fluxes are shown by thick red and blue arrows. Purple arrows depict atmospheric eddy heat transports. Eddy forced vertical motion is shown by red and blue stipples. See discussion in main text for more details.

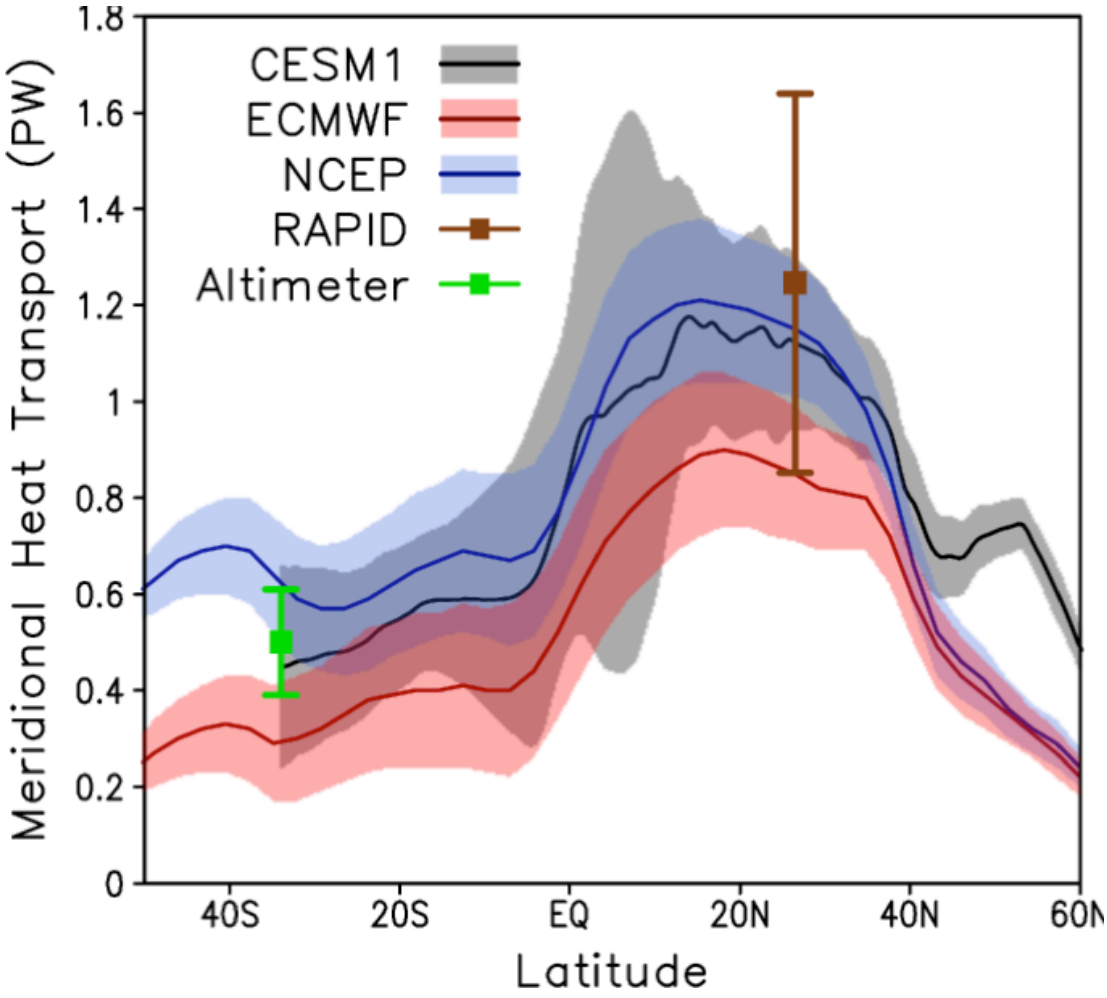

Figure 1. Meridional heat transport over the Atlantic Ocean (PetaWatts) from CESM1 model (black), gray shading represents one standard deviation. Also shown are estimated transports from NCEP (blue) and ECMWF reanalysis (red) from Trenberth et al. (2001). Direct estimates from the RAPID array at 26°N are shown in brown. Transport estimates from ARGO, XBTs, and altimetry observations at 34°S are shown by green color. The color shading and vertical bars depict one standard deviation calculated from annual average of MHT for each latitude.

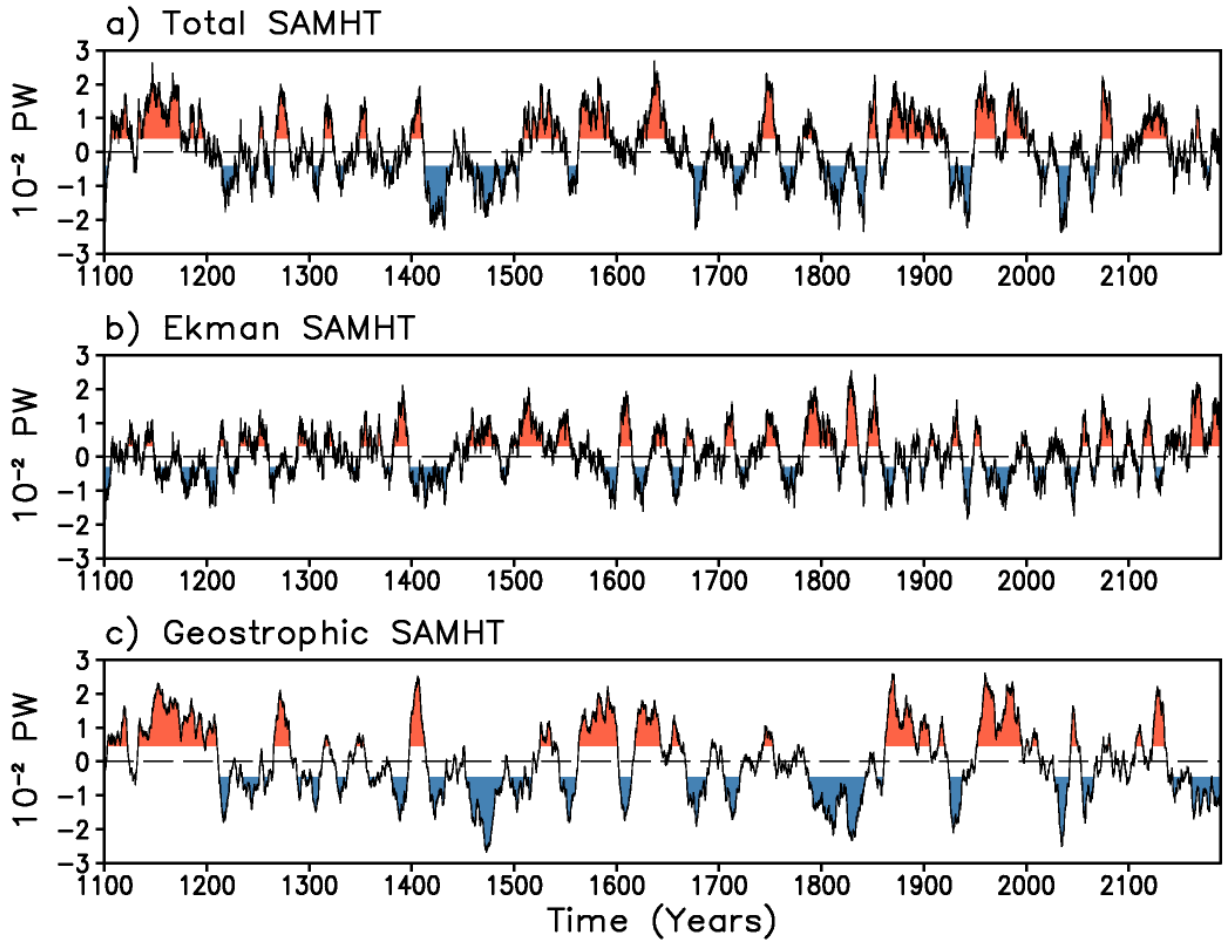

Figure 2. 11-year running average of the SAMHT timeseries for a) total, b) Ekman, and c) geostrophic component for the 1100 model year analyzed. The total timeseries is defined as the meridional heat transport at 30°S after removing the seasonal cycle and linear trend. The Ekman component is estimated using monthly mean zonal wind stress from CESM1, whereas the geostrophic term is simply taken as the difference between the total and Ekman component. The red (blue) line fill contours indicate values greater (less) than one standard deviation.

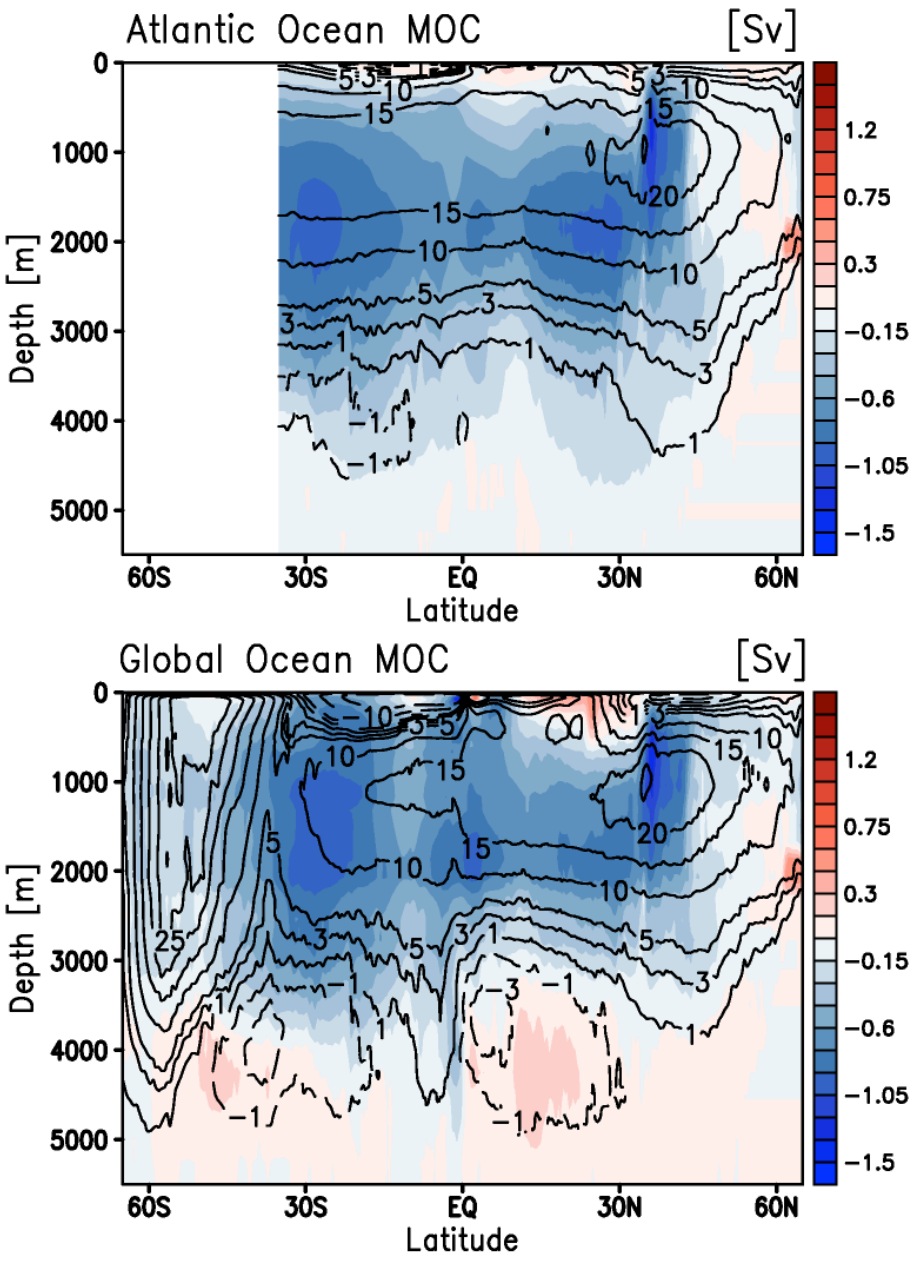

Figure 3. The mean ocean meridional overturning streamfunction for the Atlantic (top) and global ocean (bottom), where positive streamfunction indicates clockwise flow. The mean circulation is taken as the time mean, whereas the anomalous circulation is defined by the composite difference between weak minus strong SAMHT, shown by color shading.

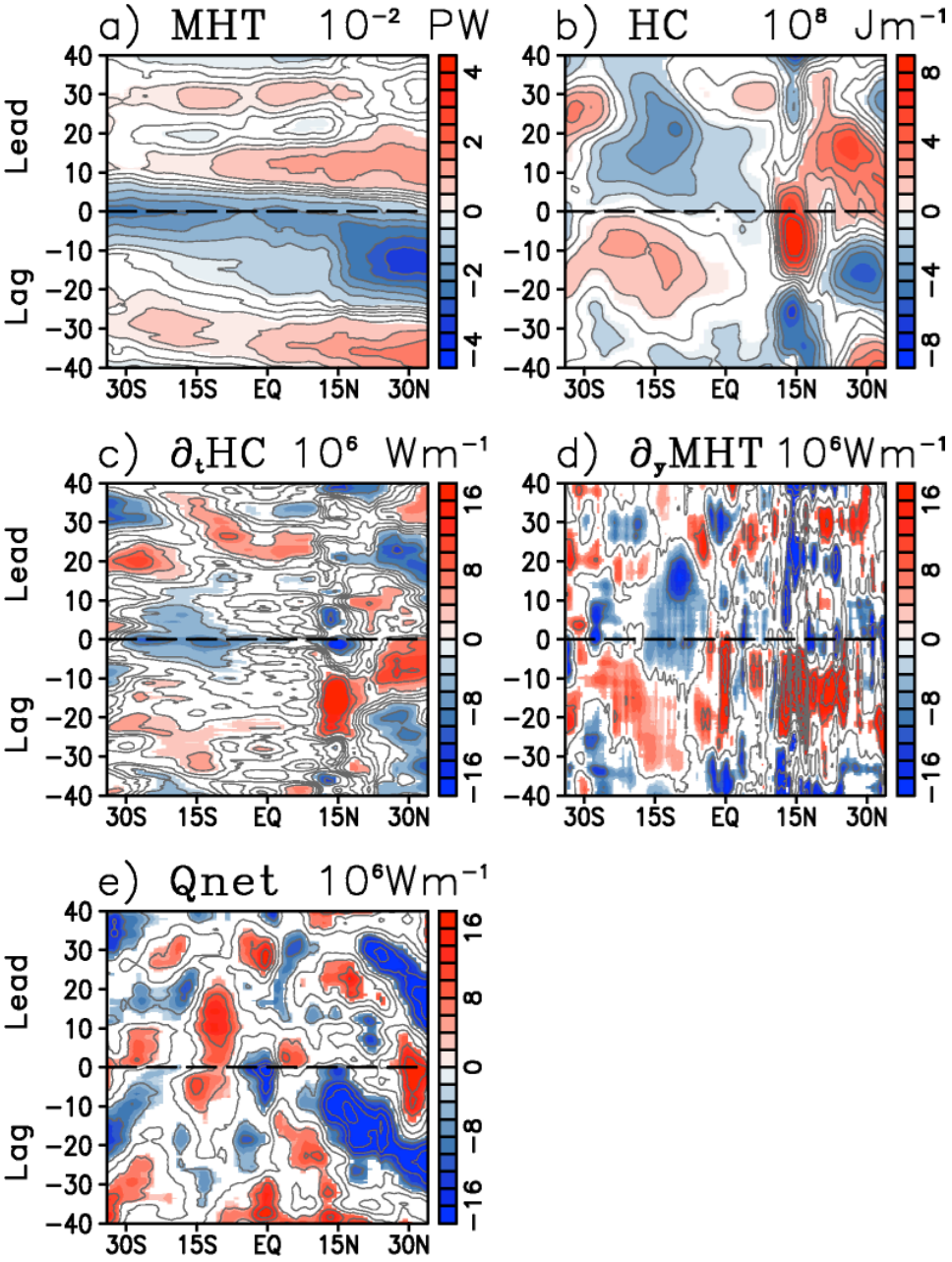

Figure 4. a) Lead-lag composite difference of zonal mean Atlantic MHT with respect to weak minus strong SAMHT. b), c), d) and e) are similar to a) but for 700m Atlantic Ocean heat content (HC), heat content tendency, MHT divergence (positive for convergence), and net surface energy flux (positive downward into the ocean) respectively. Color shading indicates 95% significance using a Kendall-tau test. The y-axis indicates time in years. Time progresses up the page with lag (lead) indicating SAMHT lags (leads), respectively.

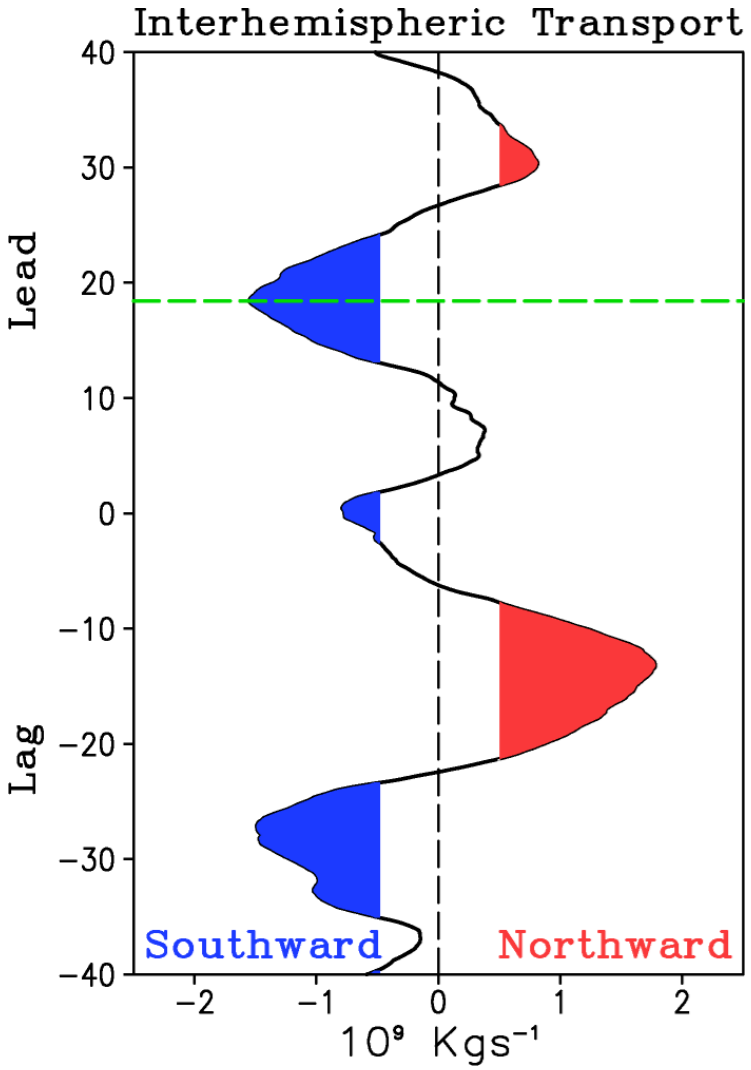

Figure 5. Lead-lag composite difference of interhemispheric atmospheric circulation depicted as the vertically integrated mass transport about the equator for weak minus strong SAMHT. Here, the direction of interhemispheric atmospheric heat transport is proportional to the mass transport with northward (southward) labeled red (blue). Color shading indicates 95% significance using a student-T test. The y-axis indicates time in years. Time progresses up the page with lag (lead) indicating that SAMHT lags (leads), respectively.

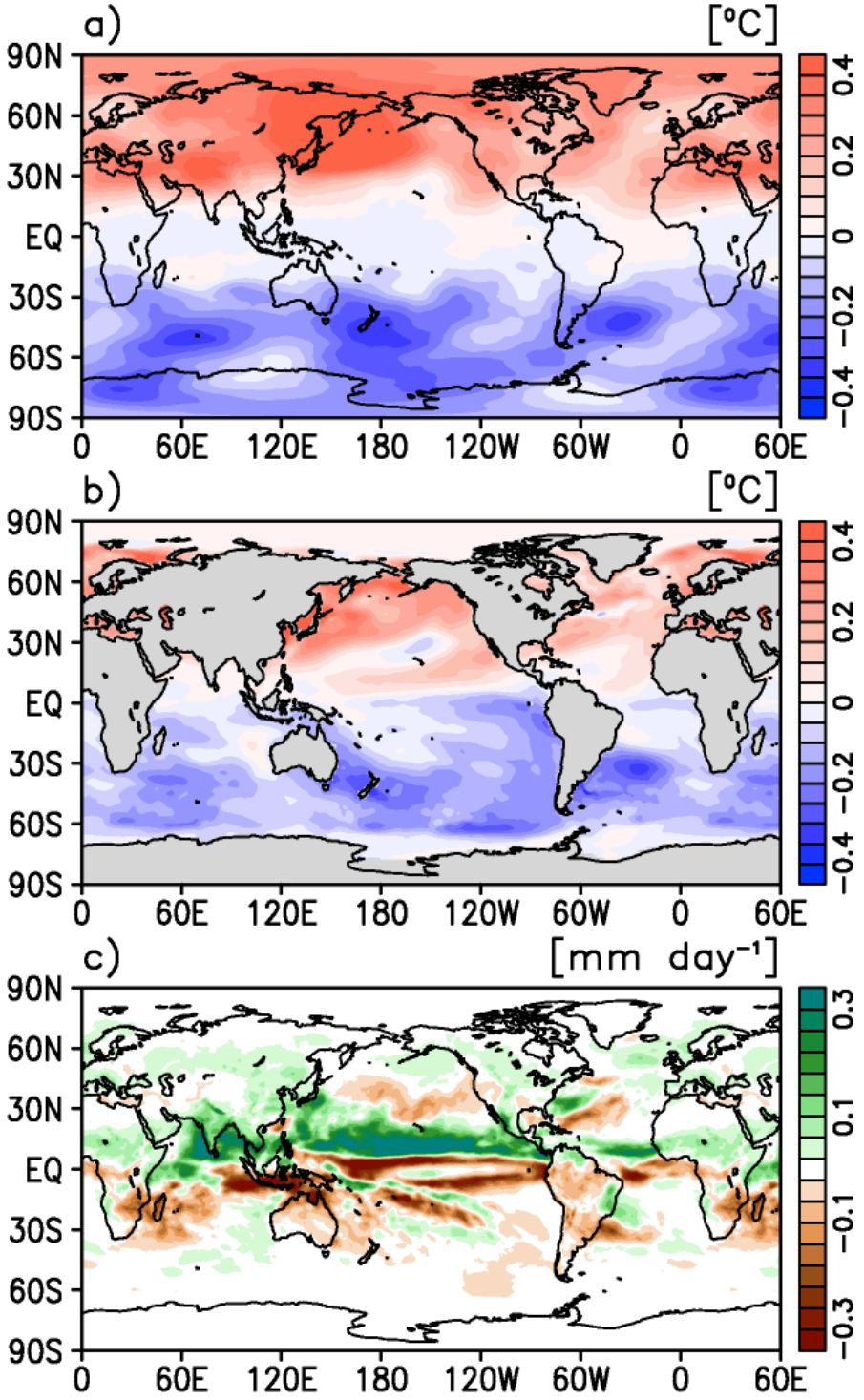

1021
1022 Figure 6. Composite difference of a) 500mb air temperature, b) sea surface temperature, and c)
1023 precipitation corresponding to weak minus strong SAMHT at 20-year lead-time (i.e., 20 years
1024 after the anomalous SAMHT.

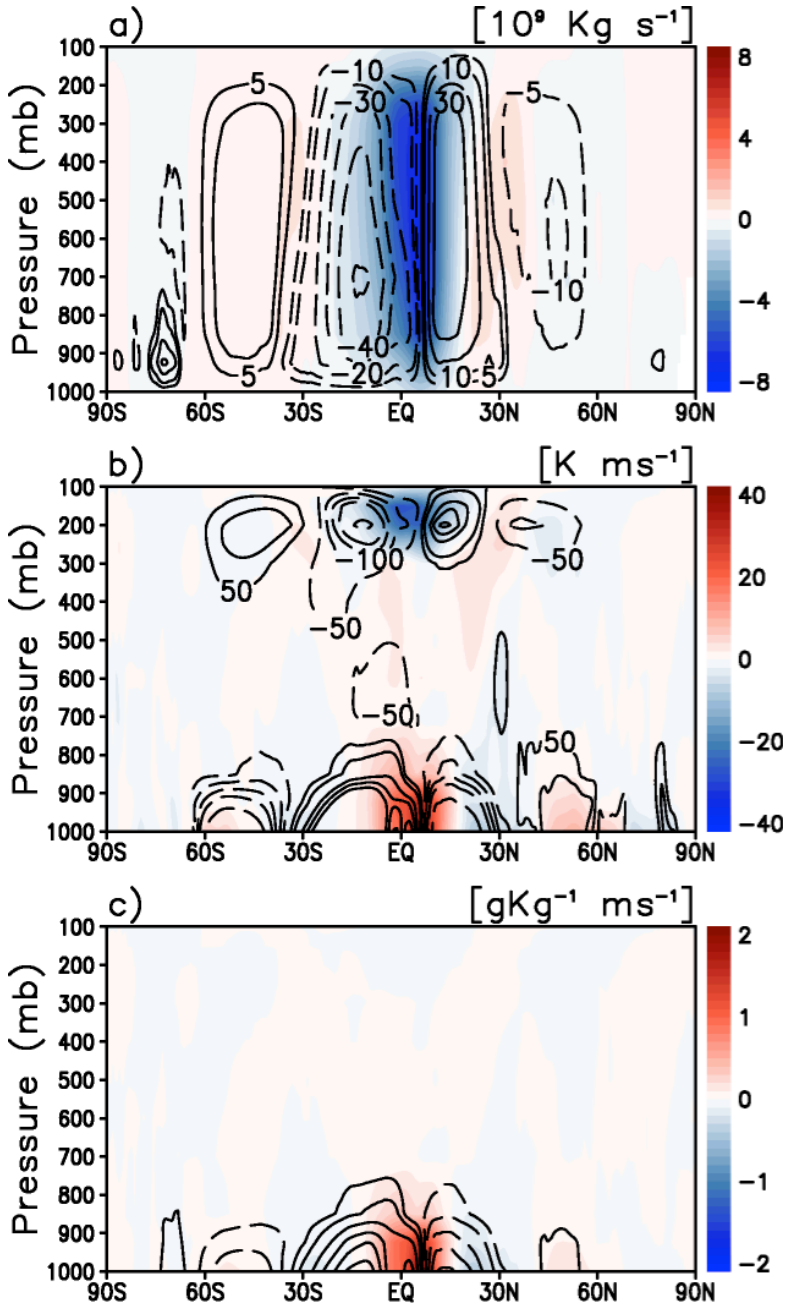

Figure 7. a) Time mean and zonal mean meridional circulation (MMC) of the atmosphere as measured by the mass streamfunction (contour) and composite difference (color) with respect to weak minus strong SAMHT at 20-year lead time (i.e., 20 years after the anomalous SAMHT, see Fig. 4). Panels b) and c) are similar to a) but for the meridional heat flux b), and meridional moisture flux c), respectively. Mean northward heat and moisture flux are indicated by positive contours and positive shading depicts anomalous northward fluxes.

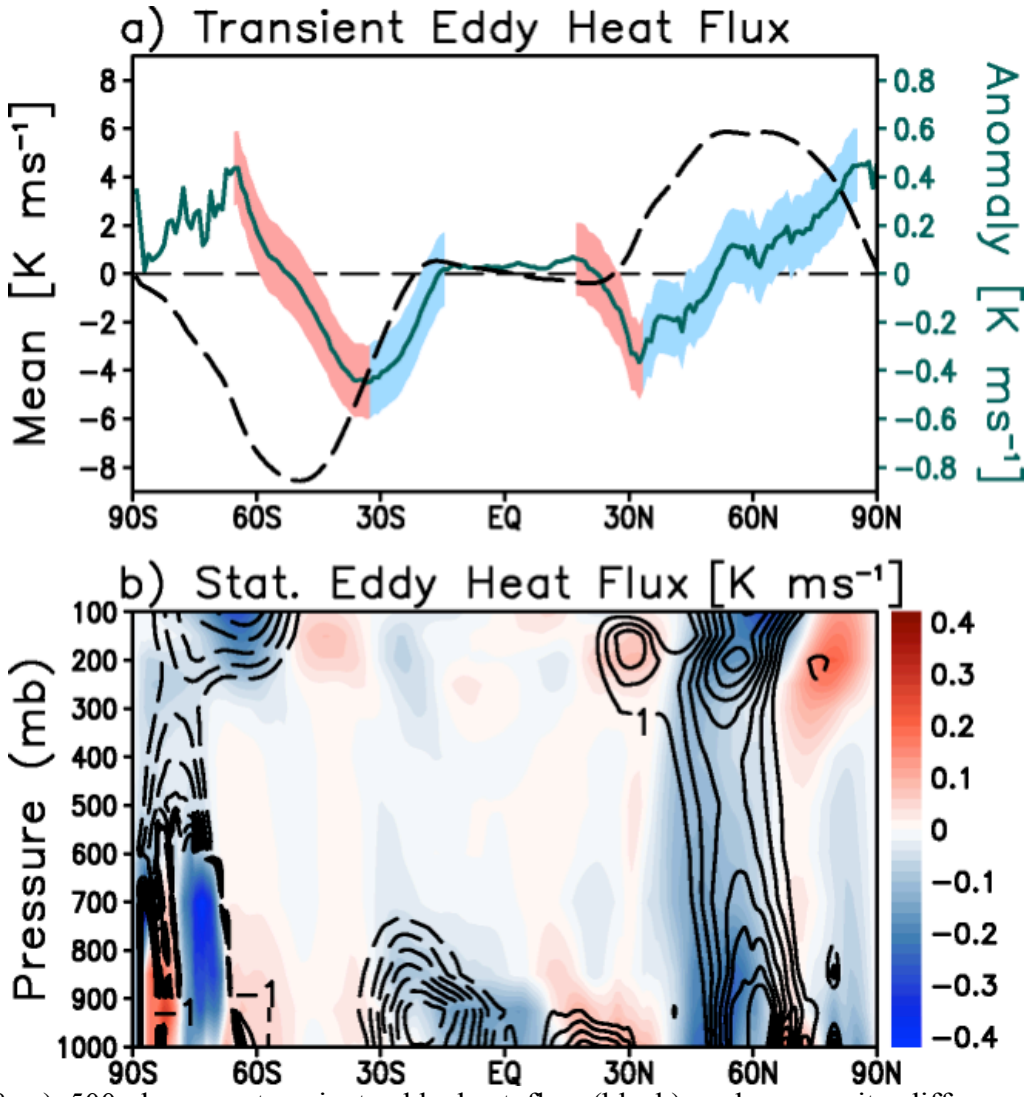

Figure 8. a) 500mb mean transient eddy heat flux (black) and composite difference (green) during weak minus strong SAMHT. Anomalous heat flux convergence (divergence) is highlighted by red (blue) regions on the composite difference line. b) Stationary eddy heat flux (black contour) and composite difference (color shading) during weak minus strong SAMHT. Similar to Fig. 7, the composite difference is analyzed 20 years after the anomalous SAMHT.

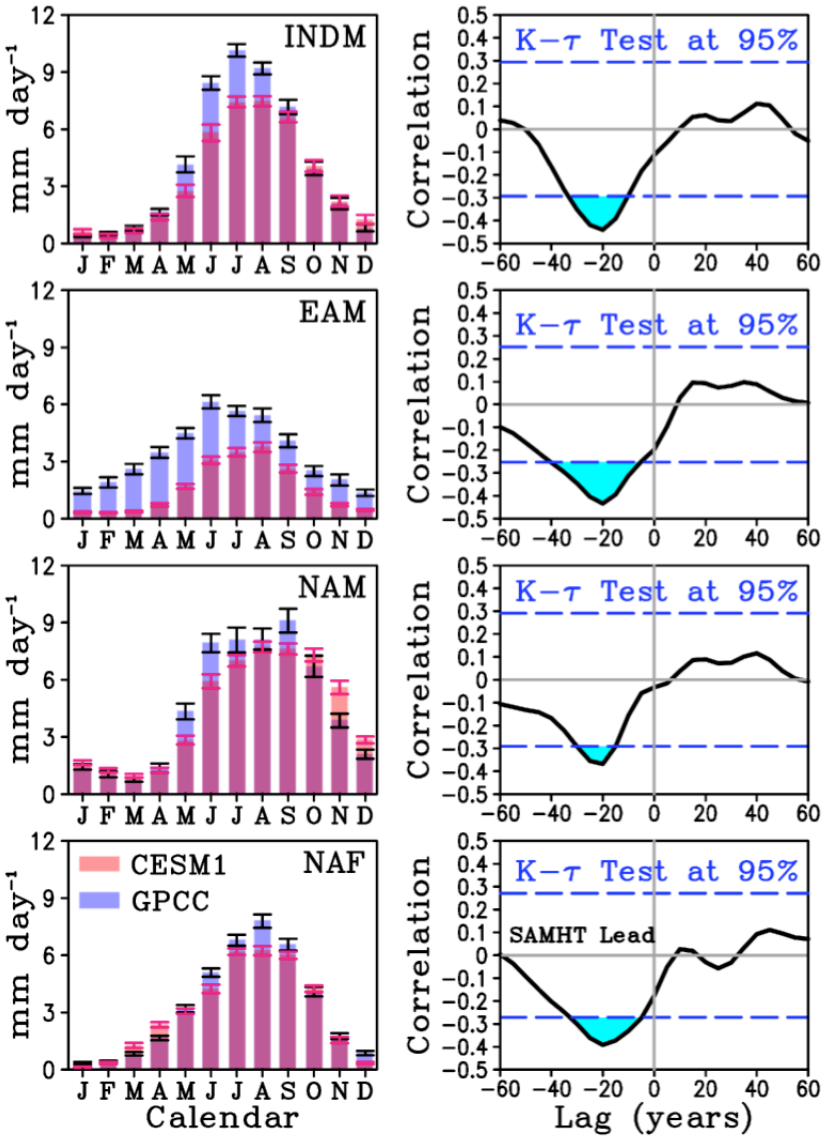

Figure 9. (left column) Seasonality of precipitation of the four monsoon regions (i.e., Indian (INDM), East Asian (EAM), North American (NAM), and North African Monsoon (NAF)) from GPCC (blue) and CESM1 (red). Error bars indicate the 99% confidence level. (right-column) Lag-lead Spearman ranked correlation between SAMHT and NH monsoon index. The blue dashed lines depict the 95% significance level based on a non-parametric Kendall-τ test. Negative lag indicates periods when SAMHT leads the NH monsoon index. Periods with significant correlation are shaded blue.

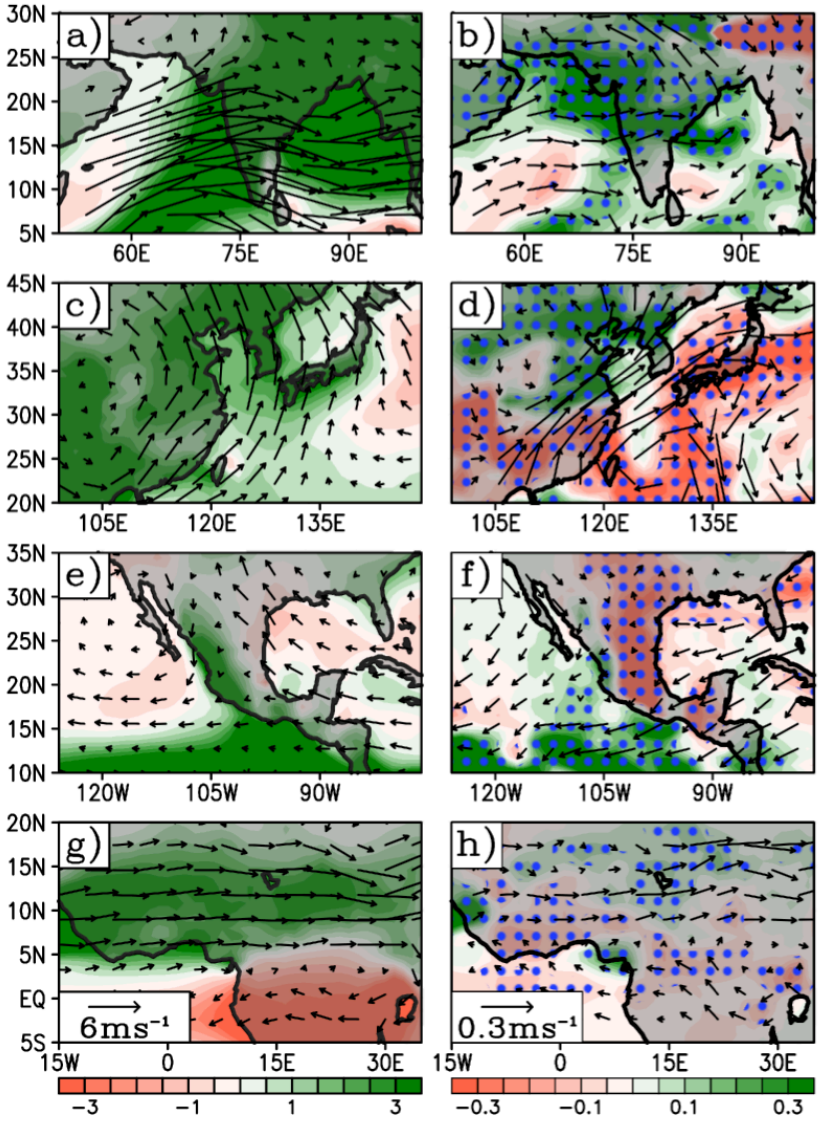

Figure 10. (left column) Seasonality of precipitation and 850mb winds for the monsoon regions (i.e., Indian (INDM), East Asian (EAM), North American (NAM), and North African Monsoon (NAF) as measured by the difference between June-July-August-September (JJAS) minus annual mean precipitation and winds. (right-column) The composite difference of JJAS precipitation (shaded) and 850mb wind for each monsoon region with respect to weak minus strong SAMHT at lead-time 20 years after the anomalous SAMHT. Blue stipples indicates regions where precipitation differences are significant at 95% confidence level based on a non-parametric Kolmogorov-Smirnov test

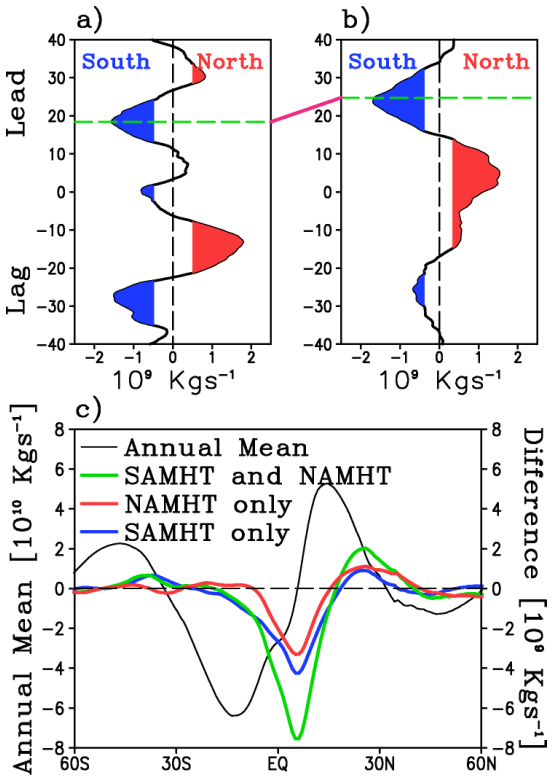

Figure 11. Anomalous interhemispheric atmospheric mass transport corresponding to a) weak minus strong SAMHT and b) weak minus strong NAMHT, similar to Fig. 5. The diagonal magenta line between panels a) and b) highlights the fact that NAMHT leads SAMHT. c) Annual mean (thin black) and composite difference of atmospheric mean meridional circulation (MMC) as measured by the zonal mean 500mb atmospheric mass streamfunction. The composite difference is centered at lead times according to that of a) and b) (dashed green lines). The conditional composite for MMC (i.e., dependent variable) is built based on the state of the SAMHT and NAMHT (i.e., independent variables). The green contour here includes the relationship between the MMC with both, SAMHT and NAMHT. Red contour depicts the relationship between NAMHT and the MMC excluding the influence of SAMHT (i.e., neutral SAMHT periods based on terciles). Similarly, blue contour shows the relationship between SAMHT and the MMC excluding the influence of NAMHT (i.e., neutral NAMHT periods based on terciles). Positive (negative) values indicate northward (southward) mass transport.

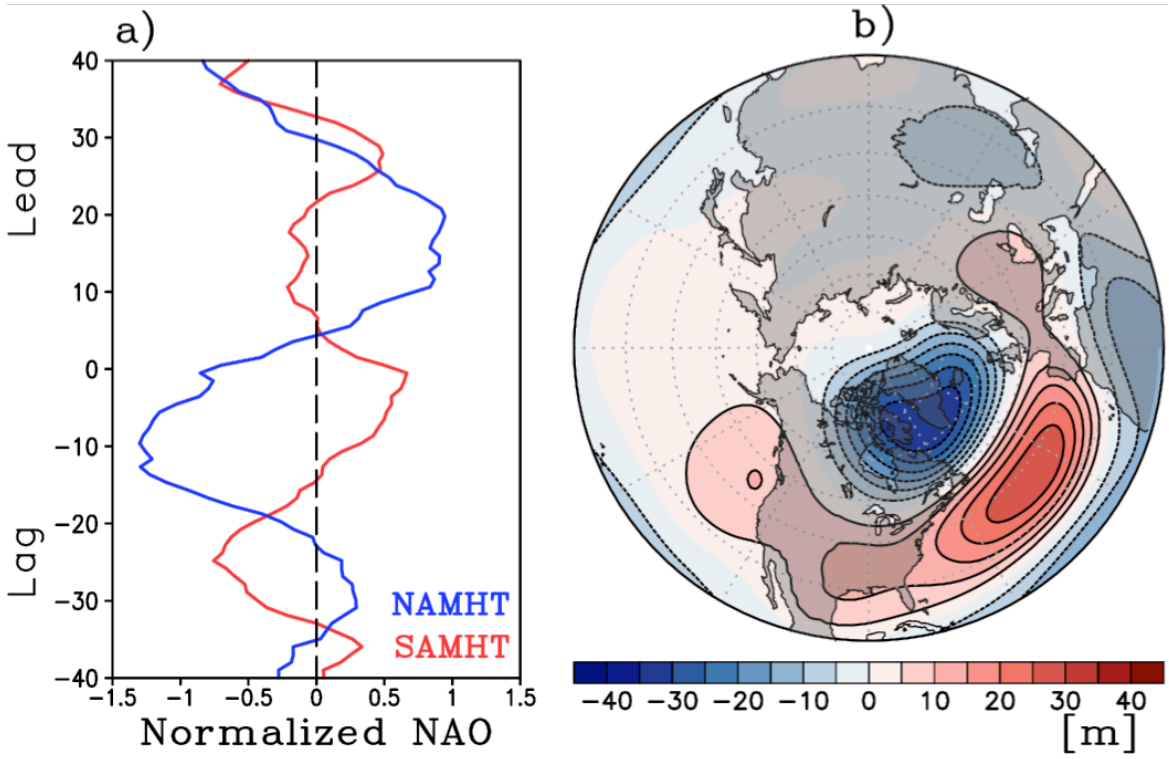

Figure 12. a) Lead-lag composite difference of North Atlantic Oscillator (NAO) index for weak minus strong SAMHT (red) and weak minus strong NAMHT (blue). The y-axis indicates time in years. Time progresses up the page with lag (lead) indicating the ocean MHT lags (leads), respectively. b) 500mb geopotential height anomaly associated with the positive phase of the NAO.

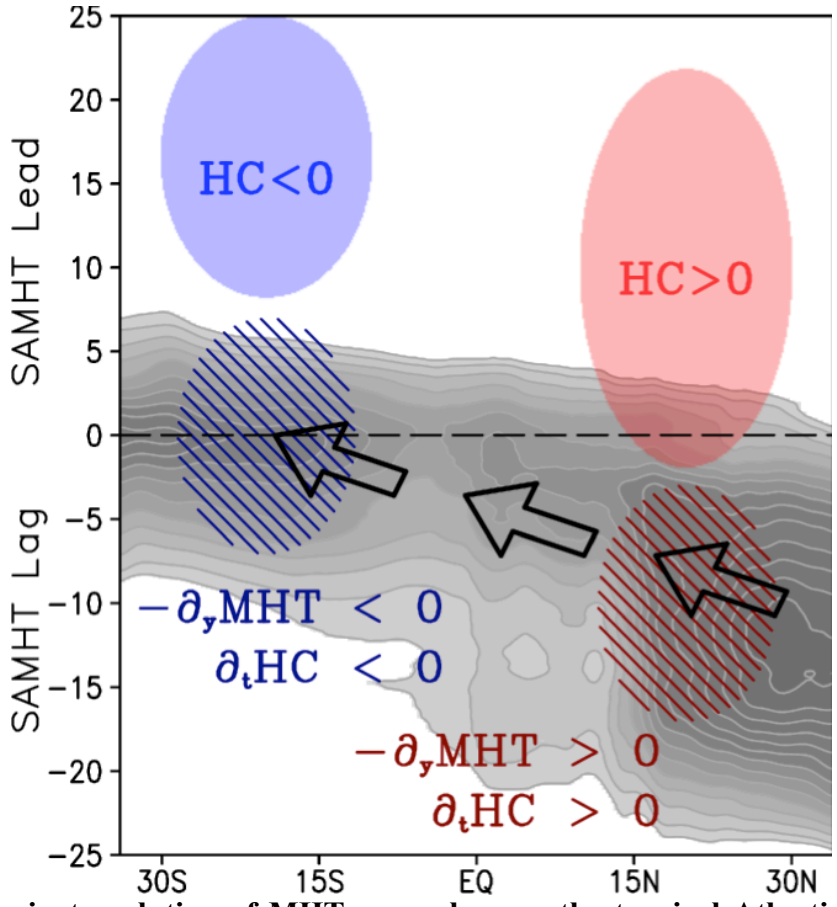

Figure 13. **Transient evolution of MHT anomaly over the tropical Atlantic Ocean during weak minus strong SAMHT.** Gray shading indicates the anomalous negative MHT (i.e., weakening of the northward heat transport). The anomaly propagates from north to south (black arrows) at about 600km/year. The dark-red hatched region indicates meridional heat transport convergence and positive heat content tendency north of the equator 10-15 years prior to the weak minus strong SAMHT, whereas the dark-blue hatched region indicates meridional heat transport divergence and negative heat content tendency south of the equator near 0-lag with respect to weak minus strong SAMHT. Blue (red) shading depicts negative (positive) heat content. The y-axis indicates time in years. Time progresses up the page, with lag (lead) indicating SAMHT lags (leads), respectively. Anomalous heat content occurs about 15-20 years after the anomalous heat content tendency and heat transport divergence in both hemispheres.

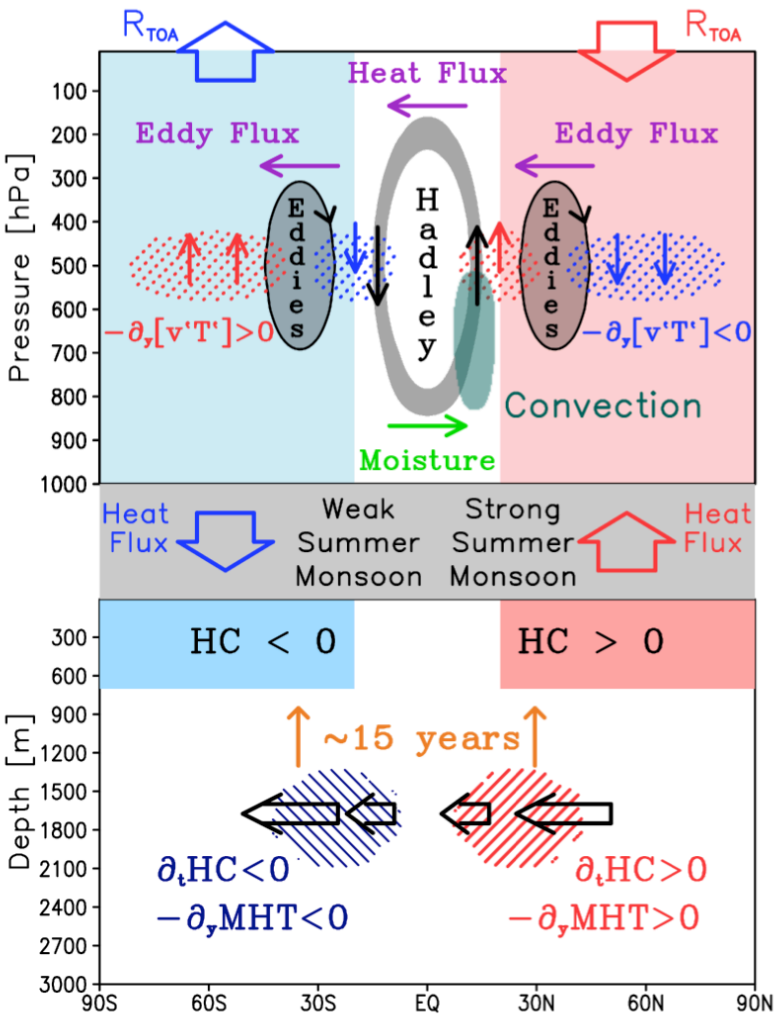

Figure 14. **Schematic diagram of the role of weaker-than-normal MHT in the anomalous atmospheric circulation at 15-20 years lead-time.** Weakened MHT is shown by thick black arrows on the bottom panel. Negative (positive) tendency in heat content is labeled by dark-blue (red) hatching. There is negative (positive) heat content in the SH (NH) about 15-20 years after the heat transport anomaly labeled here by blue (red) rectangle. Anomalous Hadley circulation is labeled by gray oval and counterclockwise circulation. Moisture and heat fluxes are shown by green and purple arrows, respectively. The TOA and surface radiative fluxes are shown by thick red and blue arrows. Purple arrows depict atmospheric eddy heat transports. Eddy forced vertical motion is shown by red and blue stipples. See discussion in main text for more details.